MATHEMATICAL MODELING OF THE EFFECTS OF WNT-10B ON BONE METABOLISM

By

CARLEY V. COOK
Bachelor of Science in Chemical Engineering.
Oklahoma State University
Stillwater, OK
2019

Submitted to the Faculty of the
Graduate College of
Oklahoma State University
in partial fulfillment of
the requirements for
the Degree of
MASTER OF SCIENCE
December, 2020

MATHEMATICAL MODELING OF THE

EFFECTS OF WNT-10B ON BONE METABOLISM

Thesis Approved:

Dr. Ashlee Ford Versypt

Thesis Advisor

Dr. Josh Ramsey

Dr. Brenda Smith

ACKNOWLEDGMENTS

To my adviser, lab mates, family, and friends who all had to listen to me babble on about my project for the past year and a half, your patience as been much appreciated and instrumental to the completion of this project. I will be forever grateful for your presence in my life.

Acknowledgments reflect the views of the author and are not endorsed by committee members or Oklahoma State University.

Name: Carley Cook

Date of Degree: December, 2020

Title of Study: MATHEMATICAL MODELING OF THE EFFECTS OF WNT-10B ON BONE METABOLISM

Major Field: Chemical Engineering

Abstract: Bone health is determined by many factors including bone metabolism. At any time, many bone multicellular units (BMU) are going through a remodeling cycle. Depending on different signaling factors, the cycle will end with the same amount of bone as at the beginning of the remodeling cycle (healthy) or increased or decreased amounts of bone. These changes contribute to chronic bone diseases such as osteoporosis. Osteoporosis results in brittle bones that are easily fractured. Recently immune cells have been identified as major signaling factors for this process. However, it is unclear how and to what extent they affect bone metabolism.

One strategy to better understand this phenomenon is to consider different foods or medicines that activate immune cells. Lactobacillus rhamnosus GG (LGG), for example, is a probiotic that increases butyrate production in the gut. Butyrate has been shown to indirectly increase bone density through a series of interconnected processes throughout the body that involve immune cells (Tyagi et al., 2018). One key process is the increase of Wnt-10b within the bone compartment by stimulated regulatory T cells. This process has been shown to increase bone volume.

Here, we focus on how Wnt-10b has been shown to alter osteoblastogenesis, osteoblast apoptosis rate, and osteoblast bone formation rate, which collectively lead to the increase of bone density (Wend et al., 2012). To model this change, we adapted a previously published and well-cited model of bone remodeling (Graham et al., 2013). The resulting model is a single compartment system that includes ordinary differential equations for cell types typically involved in remodeling such as osteoclasts, osteoblasts, and osteocytes and a delayed differential equation that tracks the amount of bone present at the remodeling site. Our alterations to the original model consist of extending it past a single remodeling cycle, implementing a reaction to Wnt-10b, and including a delayed relationship for the formation of the bone matrix. Three new parameters were estimated and validated using normalized data collected on mice (Bennett et al., 2005, 2007; Roser-Page et al., 2014). The values of the parameters were found using MATLAB nonlinear least-squares solver lsqcurvefit and delayed differential equation solver dde23.

The completed model connects Wnt-10b to bone metabolism. Interestingly, we find that this model predicts that osteoblast population does not change with Wnt-10b, but pre-osteoblast and osteoclast populations do. This model improves the understanding of immune cell disturbances to bone health and can help identify targets for medical intervention of bone loss.

TABLE OF CONTENTS

LIST OF TABLES

LIST OF FIGURES

CHAPTER I

Introduction

1.1 Osteoporosis

Osteoporosis is a disease characterized by decreased bone mass caused by the structural deterioration of bone tissue. Both trabecular bone, the bone found within the end of long bone and the interior of flapped bones, and cortical bone, the hard exterior of bone, are affected by this disease, but signs of osteoporosis are first shown in trabecular bone. The structure of healthy bone is a dense matrix with small pockets of space, but as osteoporosis breaks down the matrix, bone structure becomes less connected with larger pockets of space. Osteoporosis is considered primary if the bone loss is related to aging. Secondary osteoporosis is caused by many other health factors and diseases (Figure 1.1).

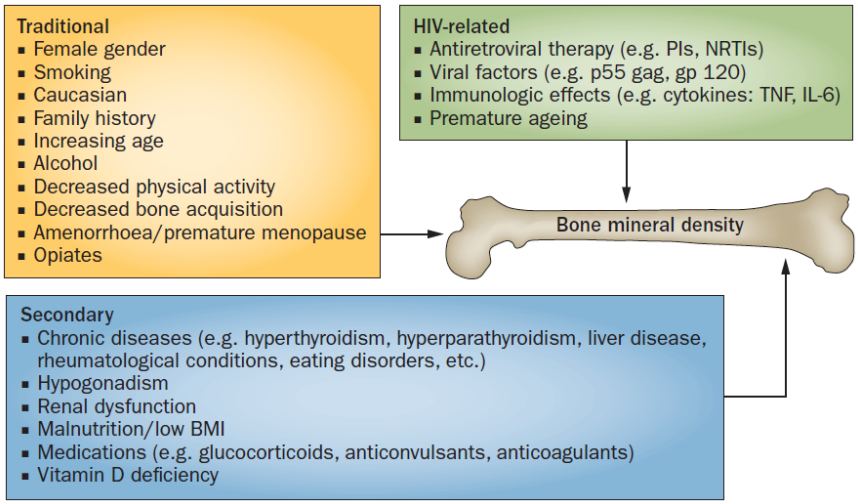

Figure 1.1: Causes of osteoporosis (Walker-Bone, 2012): Primary osteoperosis is linked to aging and other traditinal health factors such as gender, smoking, and physical activity. Secondary osteoperosis is the result of a separate underlying condition such as chronic diseases, medications, and HIV.

Over 10 million Americans age 50 or over have osteoporosis, and at least 34 million Americans are considered at risk of developing the disease. This disease results in brittle bones that are easily fractured in areas such as the wrist, hip, and spine. Many of the resulting fractures leave individuals with a lower range of mobility and a lower life expectancy. Over 1.5 million osteoporosis related fractures occur per year in the United States alone leading to a high financial burden. In 2005 the estimated cost of these fractures was 19 billion dollars (Harvey et al., 2010). Due to the prevalence of the disease and the physical and economic burden caused by the disease, understanding, preventing, and treating osteoporosis is a high priority for many research agencies.

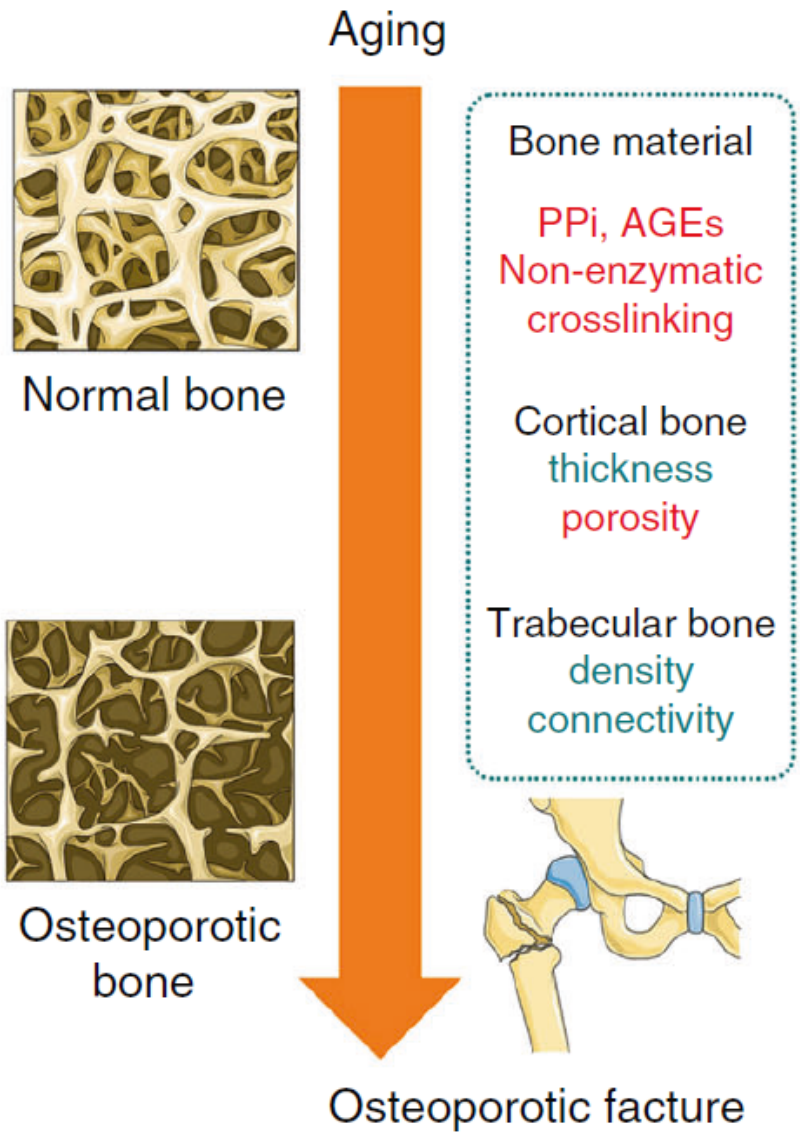

Figure 1.2: Osteoporotic fractures (Xie et al., 2019): Bone changes caused by osteoporosis lead to a higher risk of fractures. As individuals age the cortical bone begins to lose thickness and porosity, and trebecular bone material begins to lose density and connectivity resulting in an overall loss of structural integrity. This leads to inorganic pyrophosphate (PPi) and advanced glycation end-products (AGEs) accumulating in the bone.

1.2 Bone Metabolism

Bone metabolism is the process that replenishes existing bone tissue with new tissue.

The process occurs in a continuous cyclic pattern throughout an individual's lifetime

and is controlled by many complex interactions. Homeostasis or no net change in volume or density of bone is achieved when the interactions are balanced between degradation and formation. When the balance is perturbed, bone tissue no longer remodels properly, leading to weak brittle bones if bone resorption dominates (Figure 1.3).

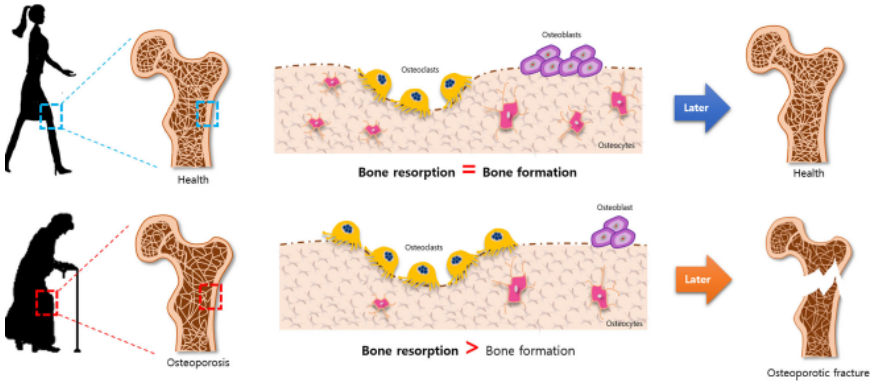

Figure 1.3: Balanced and unbalanced bone metabolism (Chang et al., 2019):(Top) A balanced remodeling cycle is when the resorption of bone equals the formation of bone. This cycle will end in no net change to the bone matrix. (Bottom) An unbalanced remodeling cycle is when the resorption of bone is greater than the bone formation. This results in a net reduction of bone mass. The less frequent case of net bone growth is not shown.

Bone metabolism works in a cyclic pattern frequently called the bone remodeling cycle (Figure 1.4). The cells involved in remodeling are part of what is called a basic mulitcellular unit (BMU). For trabecular bone the BMU works on the surface of the bone. The four main cells in a BMU are osteoclasts, pre-osteoblasts, osteoblasts, and osteocytes. Osteoclasts are responsible for breaking down the mineralized bone matrix in the resorption phase; they are differentiated from myeloid cells when the remodeling process is triggered. Pre-osteoblasts and osteoblasts are developed from mesenchymal stem cells. The difference between the two cell types is that the osteoblasts have received the proper signal to begin to rebuild the bone matrix in the formation phase, while pre-osteoblasts are still inactive in the reversal and formation phase. Osteocytes are a form of osteoblasts that have been embedded in the bone matrix during the termination phase. When these cells become damaged or die they

release a signal that triggers a remodeling cycle (Parfitt, 2002, 1994; Eriksen, 2010; Raggatt and Partridge, 2010).

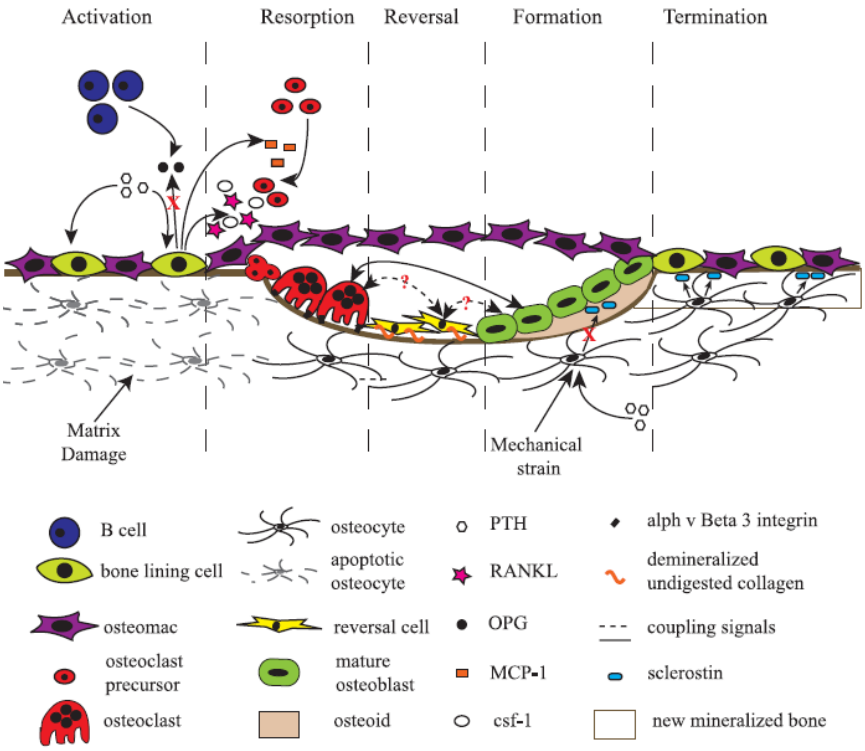

Figure 1.4: Bone remodeling phases (Raggatt and Partridge, 2010): In the activation phase the faded osteocytes represent the matrix damage that signals a remodeling cycle through chemicals such as osteoprotegerin (OPG) and macrophage colony-stimulating factor 1 (csf-1) and monocyte chemoattractant protein-1(MCP-1). During the resorption phase, osteoclasts develop due the signaling with parathyroid hormone (PTH) and receptor activator of nuclear factor $\kappa\beta$ ligand (RANKL). These osteoclasts break down that bone and are regulated by internal signaling and osteoblast signaling. The reversal phase prepares the bone surface for new bone tissue. New bone tissue is formed by mature osteoblasts during the formation phase. This phase includes pre-osteoblasts differentiating into mature osteoblasts (not shown) and mature osteoblasts embedding into the matrix as osteocytes. These osteocytes release sclerostin leading to the termination of the remodeling cycle.

1.3 Thesis Objective

This work aims to develop a better understanding of bone metabolism through a computational model. This work explores a potential way to shift bone metabolism away from over resorption to prevent or repair bone damage caused by osteoporosis. The model developed is a five equation system of ordinary and delayed differential equa-

tions that describes the relationship between the bone remodeling cycle and Wnt-10b. This thesis is a first step towards our lab's long term goal to create multicompartment mechanistic model that describes how bone health is impacted by the immune system.

CHAPTER II

Osteoimmunology and Related Models

2.1 Osteoimmunology

Interestingly, it has become clear that to obtain a full understanding of the bone remodeling cycle, one must also take into account the cross-talk between bone metabolism and the immune system. In 2001 the first paper using the term osteoimmunology was published (Targońska et al., 2001). This paper did not receive much attention, but the next paper published in 2002 was well-cited (Theill et al., 2002). Both papers introduced the idea that the immune system and bone metabolism have a complex interplay of interactions. Since, several papers have been published in an attempt to fill in what these interactions are exactly.

Some studies focus on two or three parts of the interaction and study how these parts interact. Sphingosine kinase 1 (SPHK1) has been shown to mediate the activation of sphingosine-1-phosphate receptor 1 (S1PR1). Activated S1PR1 signals the production of receptor activator of nuclear factor $\kappa\beta$ ligand (RANKL) production. This relationship is known as the SPHK1- S1PR1-RANKL axis (Xiao et al., 2018). The RANKL-receptor activator of nuclear factor $\kappa\beta$ (RANK)-osteoprotegerin (OPG) axis is very important for the production and activation of osteoclasts. RANKL and RANK signal the production and activation of osteoclasts while OPG acts as a receptor decoy inhibiting osteoclastogenesis (Leibbrandt and Penninger, 2008).

Others focus on one type of cell and interactions surrounding it. A well known immune cell, T cell, can be triggered by the parathyroid hormone (PTH) to either signal resorption or formation of bone depending on where the hormone binds on

the T cell (Pacifici, 2013). Dendritc cells are another type of immune cells that interact osteoblast. A study done with titanium plates found that titanium pushed the dendritic cells to mature faster than the osteoblasts could regenerate bone (Yang et al., 2019). In turn BMU cells can influence immune responses as well. It has been shown that osteoclasts participate in phagocytosis, antigen presentation, and immune modulation (Madel et al., 2019).

Several studies have been done over how different cytokines of the immune system interact with bone health mediator (Walsh et al., 2006; Croes et al., 2017; Bucher et al., 2019; Nanjundaiah et al., 2013; Jamali et al., 2013). Recently it was noted that this field was originally conceived to find the impact immune factors have on bone cells, but bone cells have also been shown to regulate the immune system in return (Ponzetti and Rucci, 2019).Due to the very complex interactions of this system, it is not surprising that osteoimmunology is still being actively studied.

2.2 Wnt-10b

Wnt-10b is a signaling protein that interacts with cells involved in maintaining bone metabolism and is also important to the immune system. This protein can be produced by a number of different cells, including osteoblasts and T cells. A change in Wnt-10b levels has been shown to alter the bone volume significantly (Kato et al., 2002; Patsch et al., 2011). Wend et al. (2012) and Jing et al. (2018) attribute Wnt-10b regulation of bone volume to a change of osteoblastogenesis, osteoblast apoptosis, and bone formation rate.

One way to explore how Wnt-10b interacts with bone metabolism is through studying immune responses. Lactobacillus rhamnosus GG (LGG) is a probiotic that has been shown to increase bone volume in mice through the increase of butyrate producing gut flora. Then through a series of reactions involving immune cells, butyrate causes T cells to produce Wnt-10b in bone marrow (Tyagi et al., 2018). Our

lab is currently developing a model that describes mechanistically how butyrate increases T-cell-produced Wnt-10b. By developing a model that shows the relationship between this produced Wnt-10b and bone volume, we can provide insight on how bone metabolism and the immune system interact. Combining these models would provide a mutlicompartment model that describes this phenomena providing an even deeper understanding of this relationship.

2.3 Computational Models

At this point in time, there are a few published mathematical/computational models on bone metabolism, but none of them provide a physiological understanding of the impact of Wnt-10b on bone health. In the early 2000s three models were developed. In one model a system of equations was developed to track the population changes of osteoblasts, osteoclasts and PTH. This model was used to explore the effect of PTH administration on the other two cell populations (Rattanakul et al., 2003). Another model was developed to describe the autocrine and paracrine interactions of osteoblasts and osteoclasts. This model consisted of three ordinary differential equations (ODEs) that tracks the cell populations as well as changes in bone mass (Komarova et al., 2003). In 2005 this model was updated to include a relationship with PTH (Komarova, 2005).

In 2010 more complex models began to be published. The model produced in Komarova et al. (2003) was expanded to include an ODE for myeloma cells and then altered to include spacial dimensions (Ayati et al., 2010). The same year a multicompartment model on the calcium homeostasis in the body was published. One of the compartments in the model is the bone compartment which also tracked some important bone dynamics (Peterson and Riggs, 2010).In 2013 an ODE model that tracks how different signals cause the development of osteoclasts and osteoblasts and a change in bone mass Graham et al. (2013). This model will be described in more

detain in section one of III. In 2014 a hybrid cellular automaton model was developed to explore the bone environment of metastatic prostate cancer (Araujo et al., 2014). Later this model was expanded to include possible treatment pathways (Cook et al., 2016). Another model was published around the same time that focused on the development of the bone collegan matrix. This model explored the mineralization lag time of osteoblasts (Komarova et al., 2015). All of these models provide insight into bone metabolism, however, none of them show a direct mechanistic relationship on how Wnt-10b alters the bone remodeling cycle. Thus the objective of this thesis is to develop a model that directly connects Wnt-10b and the remodeling cycle.

CHAPTER III

Model

We altered an existing bone homeostasis model without immune interactions (Graham et al., 2013) to include a mathematical relationship that represents how Wnt-10b interacts with bone formation. This is a single compartment model that tracks the important cells involved in the bone remodeling cycle as well as bone volume. We extended past a single remodeling cycle, added a reaction to Wnt-10b stimuli, and implemented a delayed relationship for the lag in bone matrix development. We added a reaction to a stimulus by utilizing published data to obtain parameters that were fitted utilizing MATLAB nonlinear least-squares solver lsqcurvefit and delayed differential equation solver dde23. During this process we consulted with Dr.Brenda Smith from the Department of Nutritional Sciences at Oklahoma State University to ensure that our model was not only mathematically correct but also physiologically relevant.

3.1 Graham 2013 Model

The existing model we utilized includes five ordinary differential equations that track the changes in populations of osteocytes (S), pre-osteoblasts (P), osteoblasts (B), osteoclasts (C), and in bone volume (z) (Graham et al., 2013). The model does not include an equation for the population of pre-osteoclasts. The model includes important autocrine and paracrine signaling factors that are represented by power law relationships (Figure 3.1). These relationships are described in Table 3.1. This section covers the parts of the Graham 2013 model that we did not alter.

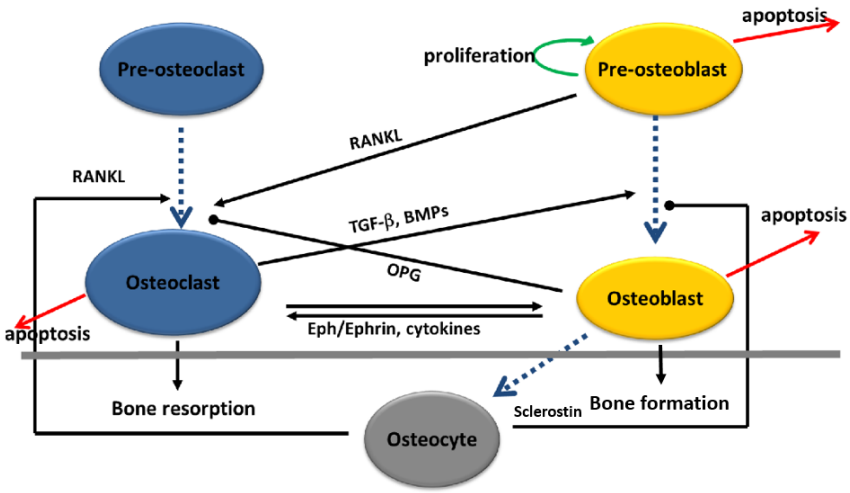

Figure 3.1: Interactions between bone cell populations adapted fromGraham et al. (2013): This figure depicts the relationships used to to develop the equations found in Graham et al. (2013). Note that only osteocytes, pre-osteoblasts, osteoblasts, and osteoclasts circles represent a differential equation. The fifth equation comes from a combination of the bone resorption and formation arrows. The other solid arrows represent autocrine and paracrine signaling factors. The dashed lines represent the transformation of one cell type to another.

3.1.1 Osteocytes

Equation 3.1 describes the dynamics of the osteocyte cell population, S. The equation shows that mature osteoblasts convert into osteocytes at a rate of α_1. The term $\left(1 - \frac{S}{K_s}\right)_+$ represents the effectiveness of sclerostin regulation by osteocytes where the $+$ means that the value must remain greater than or equal to zero. Note that although sclerostin regulation does include a Wnt pathway, we are focusing on Wnt-10b excreted from T cells or from a genetic perturbation, not Wnt-10b produced within a balanced remodeling cycle. It is assumed in the model that over the duration of remodeling, ostoecytes will not will not die; therefore, there is no death term in the equation. Instead of a death term,the osteocyte population is reduced from the steady state value of 200 cells to 180 cells at the start of each remodeling cycle. This decrease in osteocyte population represents the initial biomechanical action that

triggers a remodeling cycle.

$$\frac{dS}{dt} = \alpha_1 B^{g_{31}} \left(1 - \frac{S}{K_s}\right)_+ \tag{3.1}$$

3.1.2 Osteoclasts

Equation 3.2 describes the dynamics of the osteoclast cell population, C. It is assumed that there is large amount of pre-osteoclasts available leading to no significant change in the population so the population is not modeled. The production of osteoclasts depends on a differentiation rate, α_4 and a RANK/RANKL/OPG interaction that this described by $S^{g_{41}} P^{g_{42}} (\epsilon + B)^{g_{43}} \left(1 - \frac{S}{K_s}\right)_+^{g_{44}}$. OPG can act as a decoy receptor for RANKL. This interaction is represented as $(\epsilon + B)^{g_{43}}$. This term includes a very small number, ϵ, to prevent dividing by zero when the osteoblast population is zero since g_{43} is a negative integer. The second part of the equation shows that osteoclasts die at a rate of β_3.

$$\frac{dC}{dt} = \alpha_4 S^{g_{41}} P^{g_{42}} (\epsilon + B)^{g_{43}} \left(1 - \frac{S}{K_s}\right)_+^{g_{44}} - \beta_3 C^{f_{34}} \tag{3.2}$$

3.2 Altered Model

This section covers the parts of the model that have alterations in them. Many parts of the equations have remained the same as the Graham 2013 model, but with new terms added to each of the following equations. As these additions are related to Wnt-10b, we introduce a variable, Wnt, into the equations that represents the normalized fold change of Wnt-10b present compared to the normal levels of Wnt-10b in the system. Note that if the Wnt-10b levels are normal the remodeling cycle is normal as well and Wnt takes on a value of zero. Figure 3.2 visually describes how Wnt-10b alters the remodeling cycle.

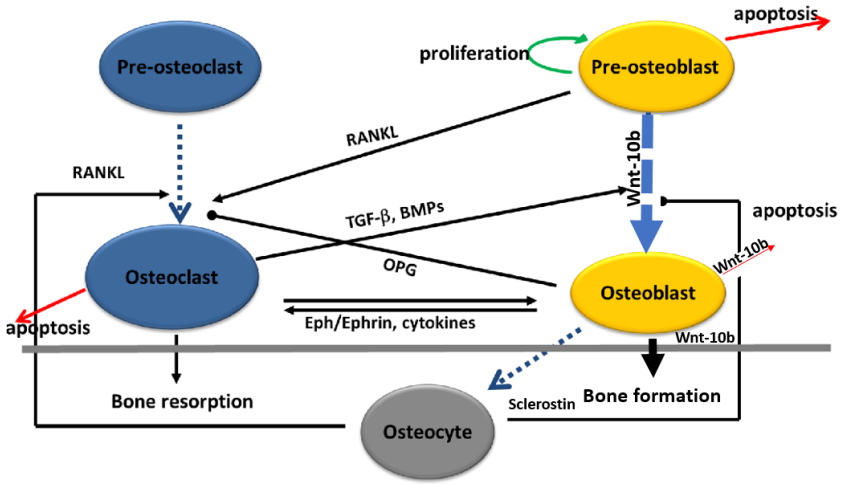

Figure 3.2: Wnt-10b alterations of bone metabolism adapted from Graham et al. (2013): Wnt-10b has a positive correlation with osteoblastogenesis and bone formation rate. Wnt-10b has a negative relationship with osteoblast apoptosis. These relationships are shown by altering the arrow size of the the original image from Graham et al. (2013).

3.2.1 Pre-Osteoblasts

Equation 3.3 describes how the pre-osteoblast cell population changes over the course of a remodeling cycle. Most of this equation has remained the same as it was in the Graham 2013 model. Pre-osteoblasts differentiate at a rate of α_2 from a large population of stem cells. This differentiation is triggered by the sclerostin signaling of osteocytes. The pre-osteoblast cell population can also be increased by proliferation of existing cells at a rate of α_3. The population can be decreased by differentiation into osteoblasts or by cell death. Cell death is represented by δP. We have altered the equation to include a linear relationship with Wnt-10b in the pre-osteoblast differentiation to osteoblast process. Pre-osteoblasts differentiate into osteoblasts at a balanced rate of β_1 due to paracrine signaling, but Wnt-10b increases this differentiation by a term of $\beta_{1adj}Wnt$.

$$\frac{dP}{dt} = \alpha_2 S^{g_{21}} \left(1 - \frac{S}{K_s}\right)_+^{g_{22}} + \alpha_3 P^{g_{32}} \left(1 - \frac{S}{K_s}\right)_+ - (\beta_1 + \beta_{1adj} Wnt) P^{f_{12}} C^{f_{14}} - \delta P \quad (3.3)$$

3.2.2 Osteoblasts

Equation 3.4 shows how osteoblasts will change over a remodeling cycle. Pre-osteoblasts mature into osteoblasts at a normal rate of β_1, but when the amount of Wnt-10b is altered, maturation rate changes by $\beta_{1adj} Wnt$ as discussed in the previous section. Wnt-10b also changes how fast osteoblasts die. This is defined as a decreasing linear relationship represented by $\beta_{2adj} Wnt$. Osteoblasts can also differentiate into osteocytes as shown by $\alpha_1 B^{g_{31}} \left(1 - \frac{S}{K_s}\right)_+$.

$$\frac{dB}{dt} = (\beta_1 + \beta_{1adj} Wnt) P^{f_{12}} C^{f_{14}} - (\beta_2 - \beta_{2adj} Wnt) B^{f_{23}} - \alpha_1 B^{g_{31}} \left(1 - \frac{S}{K_s}\right)_+ \quad (3.4)$$

3.2.3 Bone Volume

Equation 3.5 shows the dynamics of bone volume, at a single remodeling site. Bone volume is reduced by osteoclasts at a rate of k_1. This rate is slightly different than the rate in the original model due to rounding. Osteoblasts build back the bone at a balanced rate of k_2. This rate is increased by a Michaelis Menten relationship to Wnt-10b. Here half of our maximum saturation of Wnt-10b is the k_M and k_{2adj} is V_{max}. We also implemented a delayed relationship with osteoblasts to allow time for osteoblasts to build the bone matrix, as shown in Komarova et al. (2015) and Araujo et al. (2014).

$$\frac{dz}{dt} = -k_1 C + \left(k_2 + \frac{k_{2adj} Wnt}{Wnt + k_M}\right) B_{lag} \quad (3.5)$$

$$B_{lag} = B(t - \tau) \tag{3.6}$$

Table 3.1: Unaltered parameter values and definitions from Graham et al. (2013)

Parameter	Definition	Value	Units
α_1	Osteoblast embedding rate	0.5	day^{-1}
α_2	Differentiation rate of pre-osteoblast precursors	0.1	day^{-1}
α_3	Pre-osteoblast proliferation rate	0.1	day^{-1}
δ	Apoptosis of pre-osteoblasts	0.1	day^{-1}
α_4	Differentiation rate of osteoclast precursors	0.1	day^{-1}
K_s	Critical value of osteocyte population	200	cells
g_{31}	Osteoblast autocrine signaling	1	dimensionless
g_{21}	Osteocyte paracrine signaling of pre-osteoblasts	2	dimensionless
g_{22}	Sclerostin regulation of osteoblastogenesis	1	dimensionless
g_{32}	Pre-osteoblast autocrine signaling	1	dimensionless
g_{41}	Osteocyte paracrine signaling of osteoclasts	1	dimensionless
g_{42}	Pre-osteoblast paracrine signaling of osteoclasts	1	dimensionless
g_{43}	Osteoblast paracrine signaling of osteoclasts	-1	dimensionless
g_{44}	Sclerostin regulation of osteoclastogenesis	1	dimensionless
f_{12}	Pre-osteoblast paracrine signaling of osteoblasts	1	dimensionless
f_{14}	Osteoclast paracrine signaling of osteoblasts	1	dimensionless
f_{23}	Osteoblast autocrine signaling for apoptosis	1	dimensionless
f_{34}	Osteoclast autocrine signaling for apoptosis	1	dimensionless
ϵ	Avoid 0 denominator	1	cells

Table 3.2: Initial conditions for equations

Symbol	Initial Condition	Definition	Units
S	180	Osteocyte population at time t	cells
P	0	Pre-osteoblast population at time t	cells
B	0	Osteoblast population at time t	cells
C	0	Osteoclast population at time t	cells
z	100	Relative bone volume at time t	%
B_{lag}	0	Osteoblast population at time $t-\tau$	cells

Table 3.3: Adjusted parameter values and definitions from chapter IV

Parameter	Definition	Value	Units
β_1	Balanced differentiation rate of pre-osteoblasts	0.1	day^{-1}
β_{1adj}	Wnt-10b alteration of differentiation rate of pre-osteoblast	5e-03	day^{-1}
β_2	Balanced osteoblast apoptosis rate	0.1	day^{-1}
β_{2adj}	Wnt-10b alteration of osteoblast apoptosis rate	1.5e-04	day^{-1}
k_1	Bone resorption rate	0.69825	$\frac{\%\text{volume}}{\text{day}^2}$
k_2	Balanced bone formation rate	0.015445	$\frac{\%\text{volume}}{\text{day}^2}$
k_{2adj}	Wnt-10b alteration of bone formation rate	1.6828e-03	$\frac{\%\text{volume}}{\text{day}^2}$
k_M	Half saturation	25	dimensionless
τ	Time delay	14	days

Note: Estimated parameters were rounded to five significant figures based on k_2

CHAPTER IV

Developing the Model

This section covers the data used and the assumptions made in the development of this model. The parameters discussed in this section were estimated using MATLAB dde23 and lqcurvefit. At the end of each remodeling cycle the cell populations that had a value less than one was set to zero. The data shown in this section was pulled from other sources. The original tables and graphs can be found in Appendix A. If the data was originally presented in a graph then it was extracted using Plot Digitizer, a tool that digitizes the axes and gives a data point based on the pixel location. This tool helps prevent misread data points. For the purposes of our model, we took fold change to be as

$$\frac{\text{Altered levels} - \text{Baseline levels}}{\text{Baseline levels}} = \text{Fold change} \tag{4.1}$$

resulting in Figure 4.1. This was done so that the model would produce a balanced remodeling cycle when $Wnt = 0$, representing a normal baseline level of Wnt-10b. The model was used to produced a simulation with a residual norm of 154.08, which is acceptable for the values of the data, and visually fit the data well (Figure 4.2). The final parameter values can be found in Table 3.3.

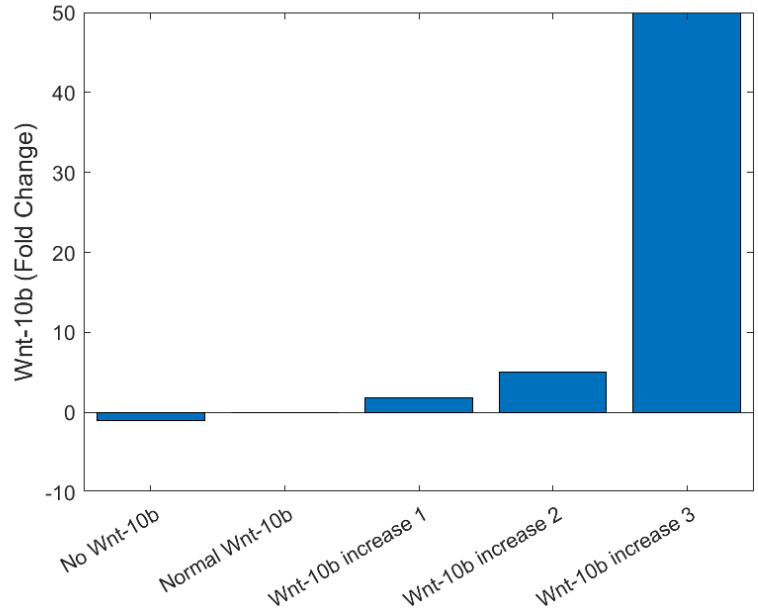

Figure 4.1: Normalized Wnt-10b fold change: The five different Wnt-10b levels are shown in bar graph form. The bars represent the normalized fold change, Wnt, of each scenario. Note that when the level of Wnt-10b is at a normal baseline the value of the bar is zero. When Wnt-10b has been deleted from the system the value of the bar becomes negative one.

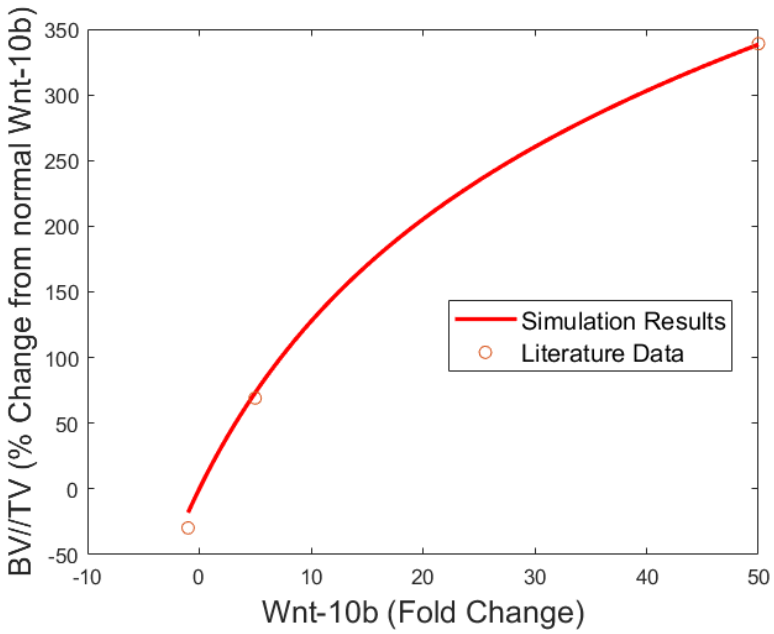

Figure 4.2: Normalized BV/TV relationship with normalized Wnt-10b fold change: The simulated results produce an acceptable residual norm of 154.08 with the data from **?** and Bennett et al. (2005). Data points were compared with the final simulated BV/TV after six remodeling cycles.

4.1 Available Data

Due to the limited amount of data on human bone remodeling, we utilized three data sources from in vivo experiments with C57BL/6 mice (Table 4.1). Two sources from the same lab were used to estimate the parameters (Bennett et al., 2005, 2007), and the third source from another lab was used to validate the model (Roser-Page et al., 2014). The BV/TV data was normalized against the control groups using

$$\frac{\text{Altered} - \text{Baseline}}{\text{Baseline}} * 100 = \text{Normalized BV/TV} \tag{4.2}$$

turning $\frac{\text{Bone Volume}}{\text{Total Volume}}$ (BV/TV) data into relative change in bone volume. In Table 4.1 "Altered BV/TV" represents mice that have been genetically altered to over or under produce Wnt-10b, while "Baseline BV/TV" represents unaltered litter mates. The normalized data was implemented into the parameter estimation code since we have a model based on human information. Note that since our model starts at a baseline of 100 percent of normal bone volume, we expect our simulation to produce z that is 100 plus the expected normalized bone volume. We also took into account the different remodeling cycle lengths of our model and mice. Mice have a 12 to 15 day remodeling cycle, but our model has a 100 day remodeling cycle (Jilka, 2013). Note that for humans a remodeling cycle is actually about 200 days long (Parfitt, 2002), but we utilized parameters from the original model that was fit for a 100 day remodeling cycle. In order for our model to show a more accurate depiction of the chronic Wnt-10b fold changes in the 3 and 6 month old mice, we extended our model to over two years of remodeling cycles. We held constant the number of remodeling cycles between mice and humans when comparing them. The mice were considered to have undergone 6 cycles. Thus we ran the computational model for humans for 6 100-day cycles. The bone volume percentage relative to baseline at the end of 6 remodeling cycles was the output compared for the parameter estimation, each stim-

ulated by different normalized Wnt-10b fold changes. The simulation results shown in Figure 4.2 are the final bone volume values after running through 6 remodeling cycles. We assumed that the 6 and 3 month old mice could be modeled at this single time point.

Table 4.1: Mice data

Normalized Wnt-10b Fold Change	Age (Months)	Altered BV/TV (%)	Baseline BV/TV (%)	Normalized BV/TV	Source
-1	3	4.3	7.4	-29.7	Bennett et al. (2007)
+1.8	3	8.04	6.35	26.6	Roser-Page et al. (2014)
+1.8	6	4.42	3.24	36.6	Roser-Page et al. (2014)
+5	3	18.1	10.7	69.2	Bennett et al. (2007)
+50	6	15.8	3.6	339	Bennett et al. (2005)

Note: Bennett et al. (2005) followed the procedures in Longo et al. (2004) to produce the fifty fold change of Wnt-10b in mice.

4.2 Parameter Estimation

As discussed in previous chapters, Wnt-10b has been shown to alter osteoblast generation, osteoblast apoptosis, and the rate of bone formation. In order to account for these changes we added three parameters $\beta_{1adj}, \beta_{2adj}$, and k_{2adj} that adjusted the corresponding relationships in the model. We also set a half saturation parameter (K_M) and a time delay (τ).

4.2.1 Osteoblast Generation

A linear relationship with Wnt-10b was chosen because it is the simplest relationship that would achieve the desired result. Knowing that literature suggested an increase

in osteoblast formation, we wanted a parameter that added to the existing β_1. To do this we chose to implement a parameter, β_{1adj}, that acted as a positive slope in the linear relationship with Wnt-10b. However, we wanted to allow for the possibility of a negative value within a logical physiological window. Knowing that $\beta_1 + \beta_{1adj}Wnt$ represents osteoblast formation we wanted to ensure that the entire term would not become negative. To do this, we solved the upper and lower bounds of the inequality

$$\beta_1 + \beta_{1adj}Wnt \geq 0 \tag{4.3}$$

using our minimum and maximum fold change in the place of the Wnt variable. The resulting -0.002 and 0.1 became bounds for the estimation of β_{1adj}. To make sure that there were no unexpected jumps or discontinuities in the model with this linear relationship, we graphed osteoblast formation in the established bounds (Figure 4.3).

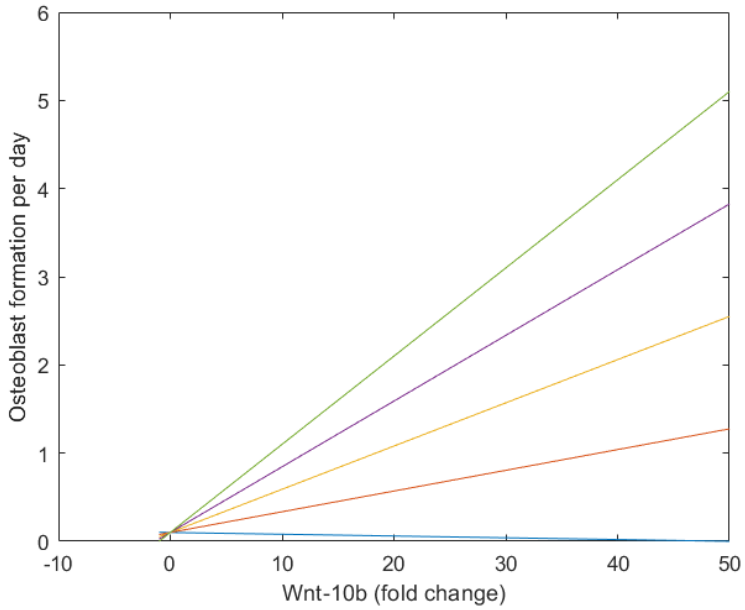

Figure 4.3: Osteoblast formation at varying values of β_{1adj} within set bounds: A positive linear relationship is expected between osteoblast formation and Wnt-10b. However, we assume that the only constraint is that the osteoblast formation must always be positive. The linear relationship is bound in such a way that our osteoblast formation per day is allow to increase or decrease with changes in Wnt-10 as long as the value remains positive.

4.2.2 Osteoblast Apoptosis

A linear relationship with Wnt-10b was also chosen for osteoblast apoptosis because it is the simplest relationship that would achieve the desired result. Knowing that literature suggested a decrease in osteoblast apoptosis, we wanted a parameter that decreased the existing β_2. To do this we chose to implement a parameter, β_{2adj}, that acted as a negative slope in the linear relationship with Wnt-10b. However, much like we did for osteoblast generation, we wanted to allow for the possibility of a positive value within a logical physiological window. Knowing that $\beta_2 - \beta_{2adj}Wnt$ represents osteoblast apoptosis, we wanted to ensure that this entire term would not become positive to do this, we solved the inequality

$$\beta_2 - \beta_{2adj}Wnt \geq 0 \tag{4.4}$$

using our minimum and maximum fold change in the place of the Wnt variable. The resulting lower (-0.1) and upper (0.002) bounds were used for the estimation of β_{2adj}. To make sure that there were no unexpected jumps or discontinuities in the model with this linear relationship we graphed osteoblast apoptosis in the established bounds (Figure 4.4).

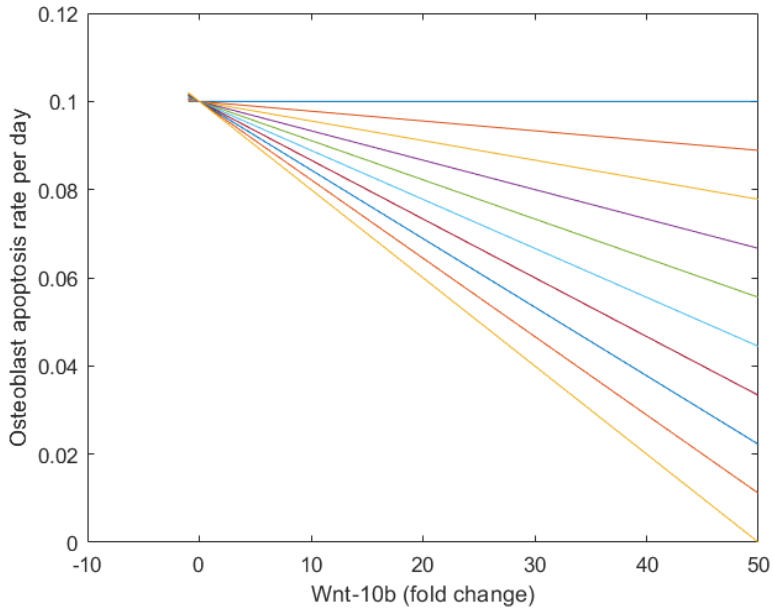

Figure 4.4: Osteoblast apoptosis at varying values of β_{2adj} within set bounds:A negative linear relationship is expected between osteoblast apoptosis and Wnt-10b. However, we initially assume that the only constraint is that the osteoblast apoptosis must always be positive. The linear relationship is bound in such a way that our osteoblast apoptosis per day is allow to increase or decrease with changes in Wnt-10 as long as the value remains positive. The top blue line is the only line that represents an increase in osteoblast apoptosis with increasing Wnt-10b.

While performing parameter estimation we began to notice a discontinuity in the relationship of Wnt-10b fold change and relative bone volume as shown in Figure 4.5. This discontinuity only occurred when β_{2adj} took on a value greater than 0.00015. It is unclear what is causing the discontinuity, but after comparing the residual norms for different β_{2adj} values as shown in Table 4.2 we set our practical upper bound to 0.00015 instead of the expected upper bound of 0.002.

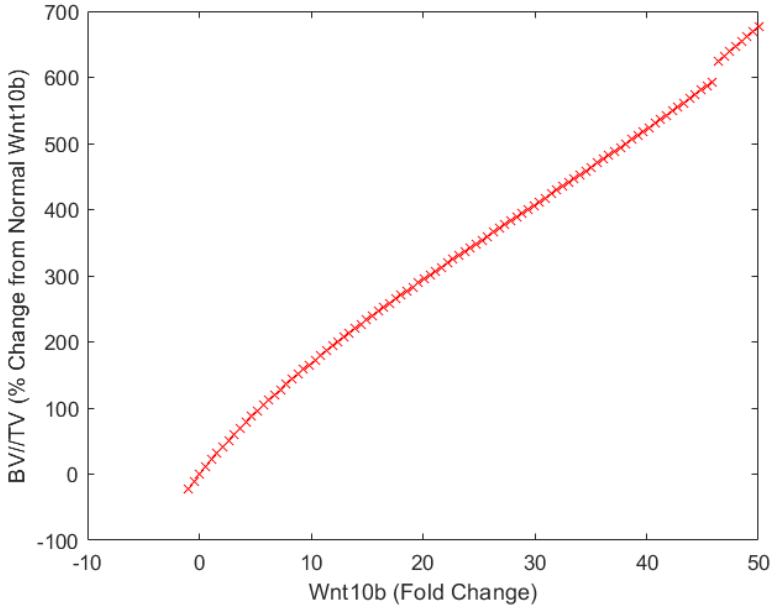

Figure 4.5: Discontinuity that occurs when β_{2adj} is greater than 0.00015: There us a jump in the estimated normalized BV/TV when β_{2adj} is greater than 0.00015. This jump indicates a discontinuity in the solution within the set bounds for β_{2adj}.

Table 4.2: Residual norms for different β_{2adj} upper bounds

β_{2adj}	Residual Norm
0.00015	154.08
0.0002	476.00
0.00075	114330
0.002	$3.97e10^7$

4.2.3 Bone Formation Rate of Osteoblast

Like the Wnt-10b relationships with osteoblast formation and apoptosis, we attempted to implement a linear relationship for the bone formation rate of osteoblast, but this resulted in high residual norms or nonphysical parameter values. We chose instead to implement a Michaelis Menten relationship. This decision was partly based on some extra data provided in Bennett et al. (2007) shown in Figure 4.6 and also partly because it produced the best residual norm with physiological parameter values. We chose only to set a lower bound of 0 with k_{2adj} because we knew from data that this needed to cause an increase of bone formation.

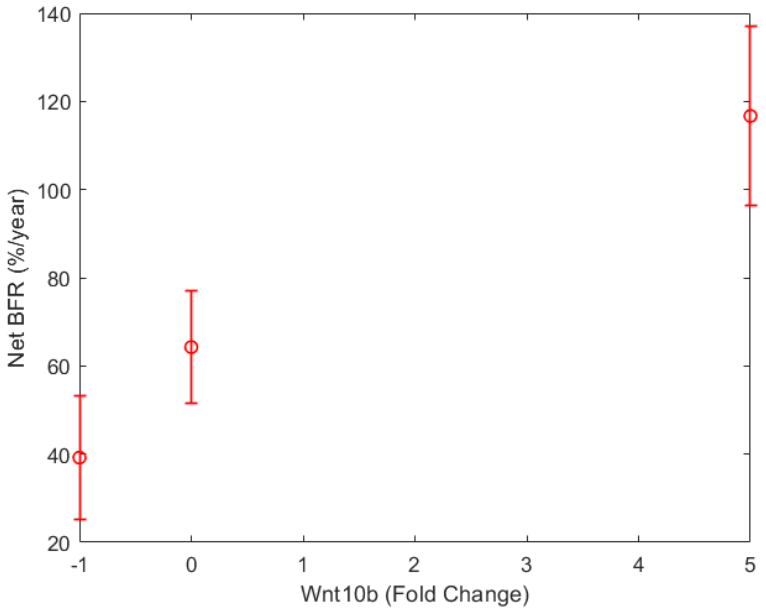

Figure 4.6: Net mouse bone formation rate (Bennett et al., 2007): The net bone formation rate (BFR) of mice was recorded in Bennett et al. (2007). When graphed this data shows a slight curve to the relationship between net BFR and normalized Wnt-10b levels. This curve is characteristic of a Michaelis Mentien relationship.

Figure 4.6 shows the change in net bone formation rate (BFR) for mice with Wnt-10b values ranging from a normalized 1 fold decrease to a normalized 5 fold increase. From the data you can see a slight curve that would be expected for a Michaelis Mentien relationship. We could not use this data for much more than a visual understanding of the relationship between bone formation and Wnt-10b, because this data does not separate out the bone formation rate from the bone resorption rate as in our model.

After deciding on a Michaelis Mentien relationship in the form of

$$BFR = (k_2 + \frac{k_{2adj} Wnt}{Wnt + k_M}) \tag{4.5}$$

for bone formation and Wnt-10b, we explored two values for k_M, 25 and 50. First, we compared the residual norms of the resulting parameter estimations, but they were very close at 154.08 and 151.32. In order to decide between them, we graphed

bone formation against Wnt-10b (Figure 4.7) and compared the shape of the curves. We decided on k_M equal to 25 because the curve was more responsive to changes in Wnt-10b indicating a stronger saturation.

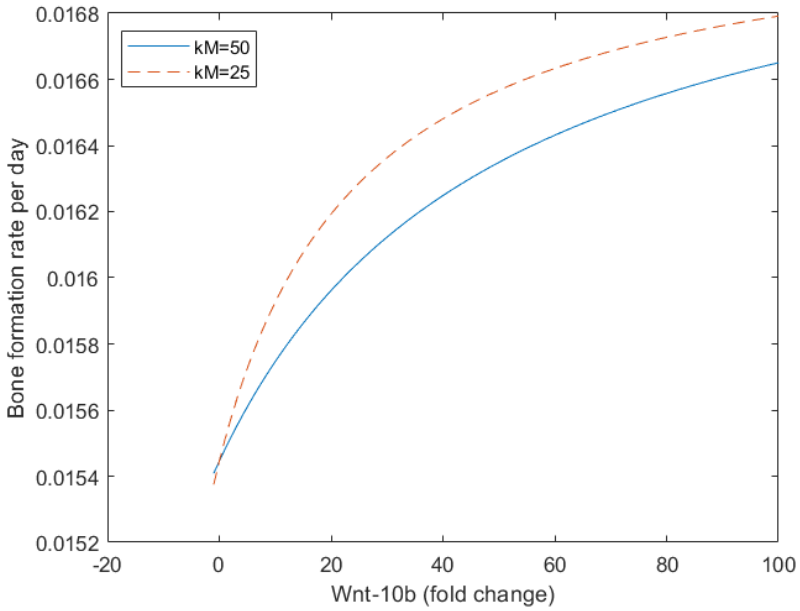

Figure 4.7: Estimated bone formation rate with varying k_M values: The BFR rate for two values of K_M are compared. When K_M is equal to 25 the BFR changes are more dramatic than when the K_M is equal to 50. This indicates that K_M equal to 25 represents a stronger saturation of Wnt-10b.

4.3 Delayed Osteoblast Activity

The results from our first few rounds of parameter estimation yielded Figure 4.8. After discussing the resulting shape of the curve with Dr.Smith, we decided that this was a nonphysical result. Bone resorption should only occur once during a remodeling cycle. To remedy this we looked at other models and literature. We found that mature osteoblasts take about 10 to 14 days to produce the bone matrix (Komarova et al., 2015; Araujo et al., 2014). This information led us to implement a delayed relationship of 14 days between the osteoblast population and the bone formation rate. This is represented by B_{lag}. After using the delayed relationship, the parameter estimation results were giving curves that looked to be more physiologically relevant

(Figure 4.9).

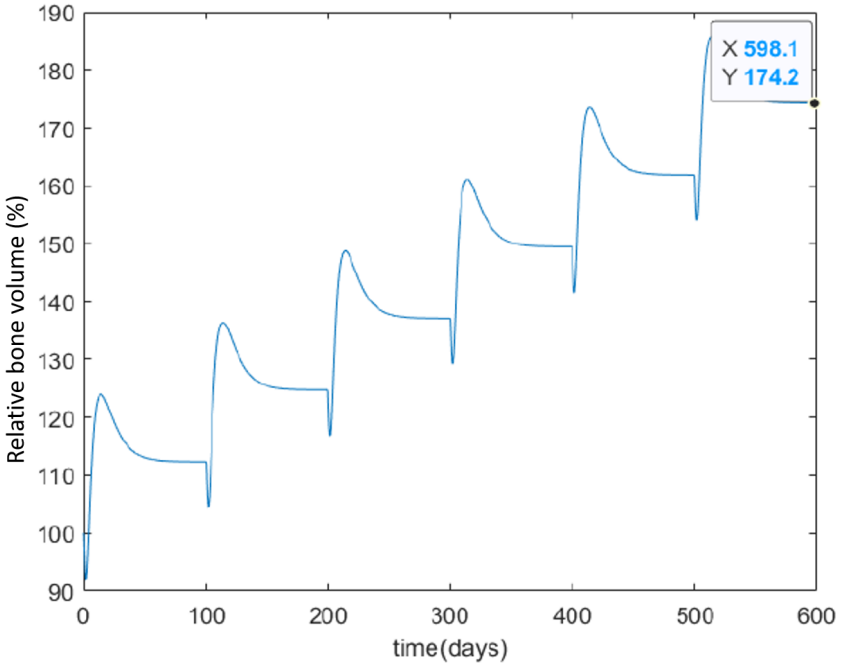

Figure 4.8: Nonphysical Bone dynamics with a 5 fold increase in Wnt-10b: The simulated curve shows the results of the initial parameter estimation. The endpoint is close to the data, but the shape of the curve is not a physical possibility. This result indicates that there are two resorption phases in a single remodeling cycle. This is not a possibility in a living system.

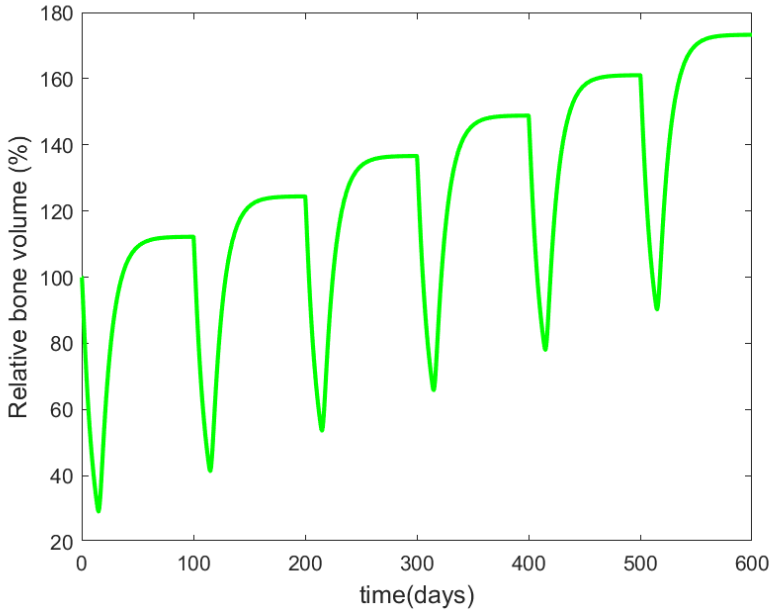

Figure 4.9: Physiologically relevant bone dynamics with a 5 fold increase in Wnt-10b: After implementing a time delay the simulation gave physiologically relevant bone dynamics. The simulation still ends close to the data and gives the expected bone remodeling cycle with one resorption and formation phase.

4.4 Bone Resorption Manual Adjustment

Another adjustment we had to make was to the value of k_1 as shown in Table 4.3. This was not due to any changes in Wnt-10b, but rather a rounding issue with the original model. Figure 4.10 shows the bone volume results from the original model (Graham et al., 2013). The cycle does not go back to 100 as expected with a balanced remodeling cycle. When we replicated the Graham 2013 model in MATLAB using the corresponding SIMBIOLOGY file, we also saw the same issue (Figure 4.11). Since Equation 3.5 depends on a resorption and formation term we looked closer at k_1 and k_2. The original value for k_1 was 0.7, but after looking at the significant figures in k_2, we decided that the authors could have rounded k_1 without noticing the slight deviation from a truly balanced cycle since they only considered one cycle. The offset after several cycles is much more significant. We manually balanced the remodeling cycle by slightly reducing the value of k_1. This process had to be repeated after the

delayed relationship with osteoblasts was implemented. As seen in Figure 4.13 the first remodeling cycle related to the delayed relationship goes up to a value of 99.99, but the remaining cycles all balance at 100. We believe that this difference is not enough to make a significant difference in the model results.

Table 4.3: Bone resorption rate values

Model	k_1
Unbalanced	0.7
Balanced	0.6983
Balanced with delay	0.69825

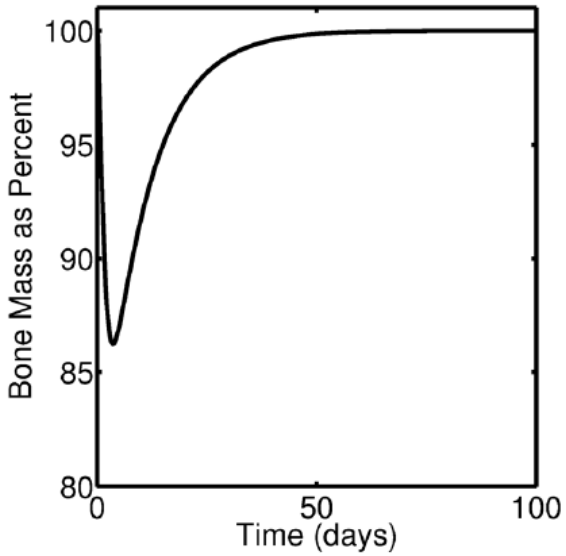

Figure 4.10: Original model results (Graham et al., 2013): The results represented in Graham et al. (2013) show that their model ends a cylce at a value just below 100 percent. This difference is barely noticeable for a single remodeling cylce.

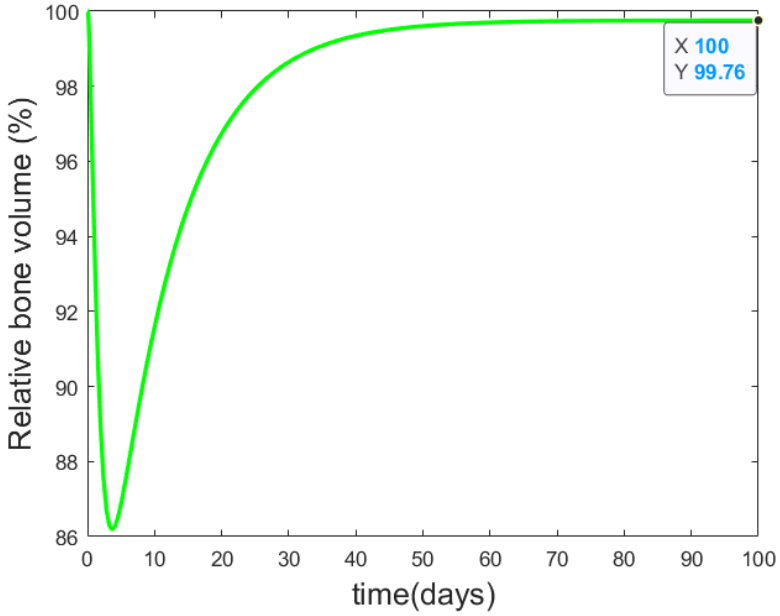

Figure 4.11: Original model replicated: The original model was replicated using a SIMBIOLOGY file. The cycle ends at 99.76 instead of the expected 100. The value for k_1 is set to 0.7. This is consistent with Figure 4.10

.

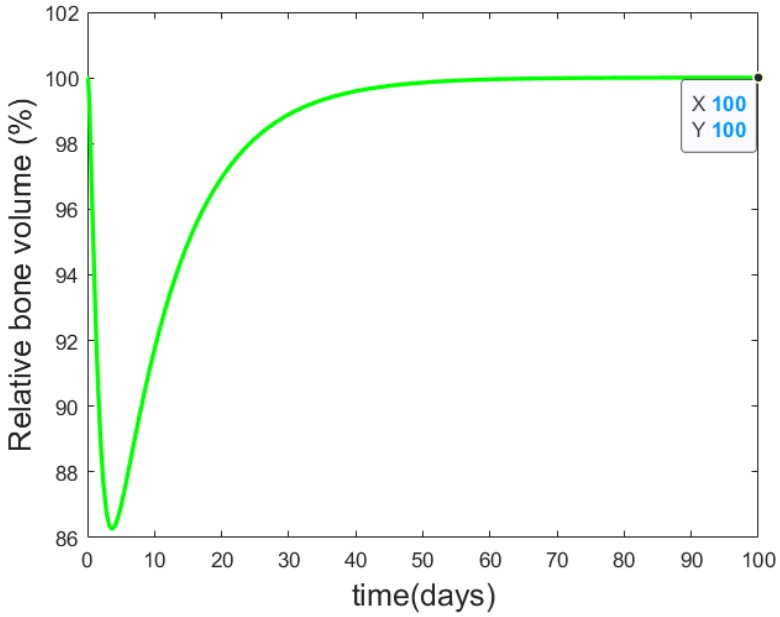

Figure 4.12: Original model balanced: When k_1 was changed to 0.6983 the cycle became balanced. The model now starts and ends at 100 percent relative bone volume.

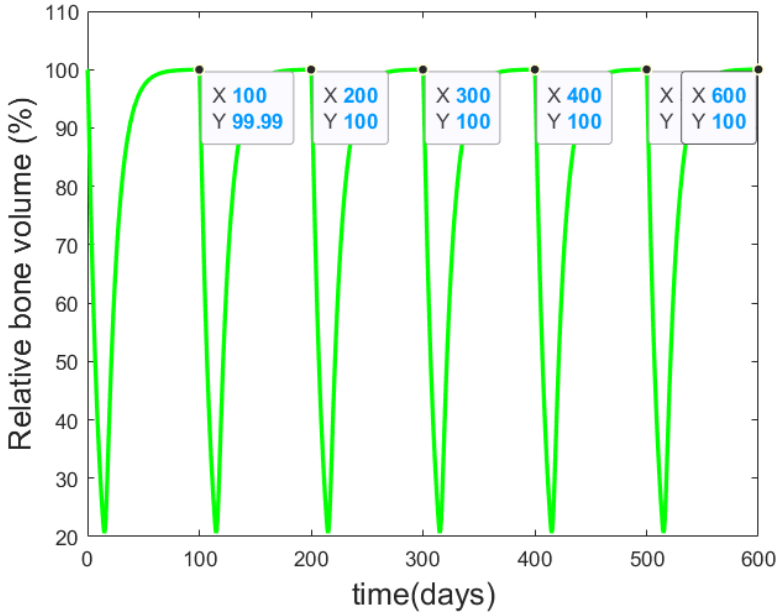

Figure 4.13: Model with delay balanced: When a delayed relationship for osteoblast bone formation was implemented, the model had to be re-balanced slightly. The final value for k_1 was set at 0.69825. This results in a slightly unbalanced initial remodeling cycle followed by completely balanced remodeling cycles.

CHAPTER V

Model Results and Validation

5.1 Model Validation

To determine if the model was a good predictor of the change in bone volume that occurs when Wnt-10b levels are altered, we utilized a separate set of data (Roser-Page et al., 2014). In Figure A.3(Appendix A), there is extra data provided on the range of the measurements taken. To produce error bars for the validation, we used

$$\frac{\pm\text{Data for Altered Case}}{\text{Altered Data}} = \text{Error Range} \tag{5.1}$$

. This relationship provided us with the smallest error. The simulation results fall within the error of the data (Figure 5.1).

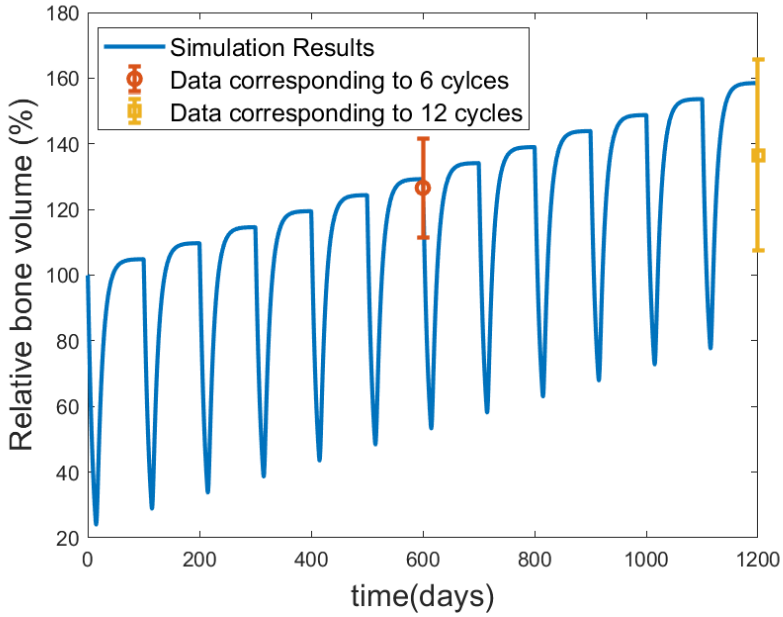

Figure 5.1: Validation of model with data from Roser-Page et al. (2014): The simulation shown is the result of running the model with a 1.8 normalized fold change of Wnt-10b for twelve remodeling cycles. The data provided in Roser-Page et al. (2014) corresponds to six and twelve remodeling cycles. The simulation falls withing the error of the data provided.

5.2 Model Results

The final validated model gives the results shown in Figure 5.2. The initial conditions for these simulations are provided in Table 3.2. As Wnt-10b increases the bone volume also increases. For each fold change in Wnt-10b shown, there is also corresponding information on the activated populations of osteocytes, pre-osteoblasts, osteoblasts, and osteoclasts (Figures 5.3, 5.4, and 5.5). Interestingly, across all three cases the activated osteoblast population seems to remain relatively consistent across all cycles even though we altered the formation and apoptosis rates for osteoblasts.

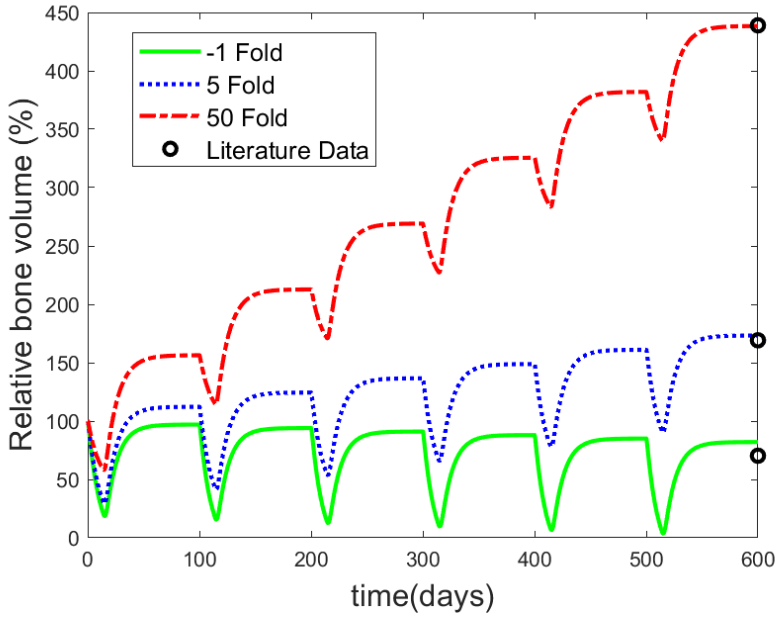

Figure 5.2: Simulation results for three normalized Wnt-10b fold changes: The different fold changes used to parameterize the model are shown with the corresponding data points from Bennett et al. (2005) and Bennett et al. (2007). All three simulations were ran for six remodeling cycles and end close to the corresponding data.

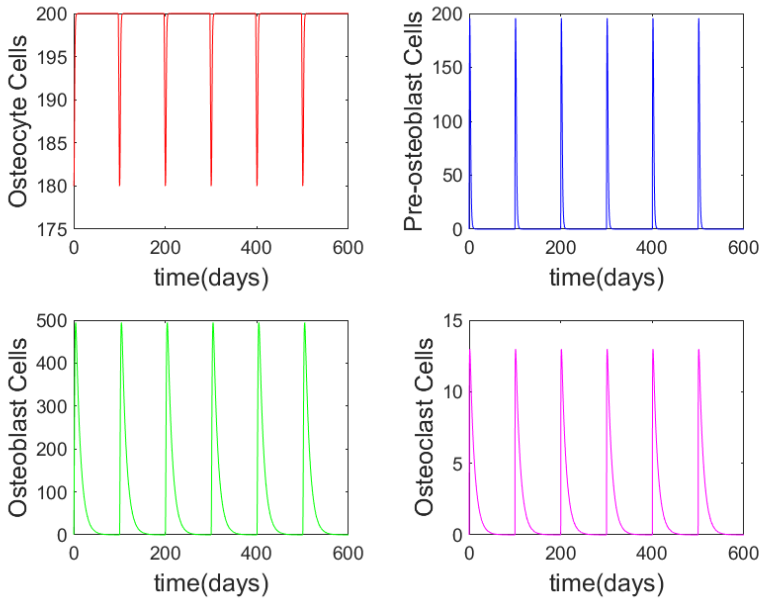

Figure 5.3: Activated cell population results for a normalized 1 fold decrease in Wnt-10b: The activated cell populations follow identical dynamics for each remodeling cycle. For osteocytes, the activated cell population is decreased at the start of a remodeling cycle and then increases back up to the steady state activated population of two hundred. The other three cells types initially increase from a steady state activated population of zero and then decrease back to zero.

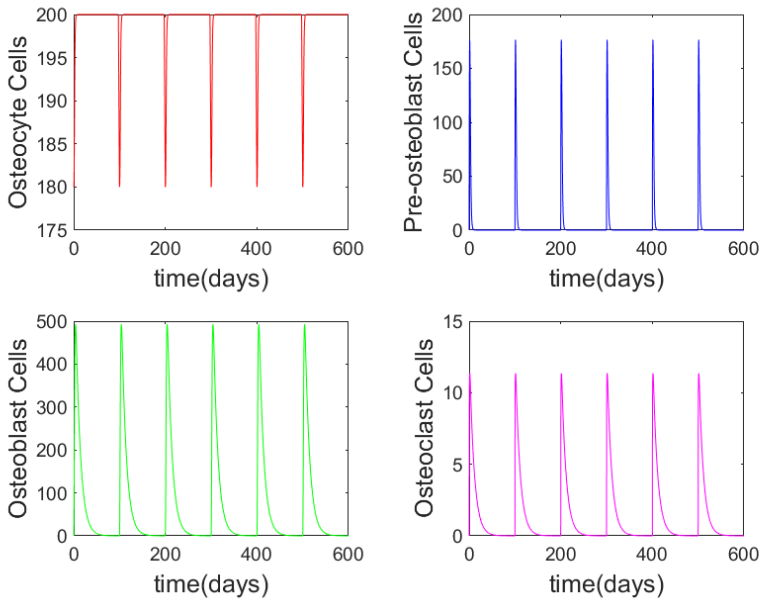

Figure 5.4: Activated cell population results for a normalized 5 fold increase in Wnt-10b: The cell dynamics for a normalized 5 fold increase in Wnt-10b follow the same pattern as the activated cell populations for a normalized 1 fold decrease in Wnt-10b (Figure 5.3). The maximum activated cell population of pre-osteoblasts and osteoclasts does decrease from the previous case. The activate osteoblast and osteocyte populations remain consistent with the previous case.

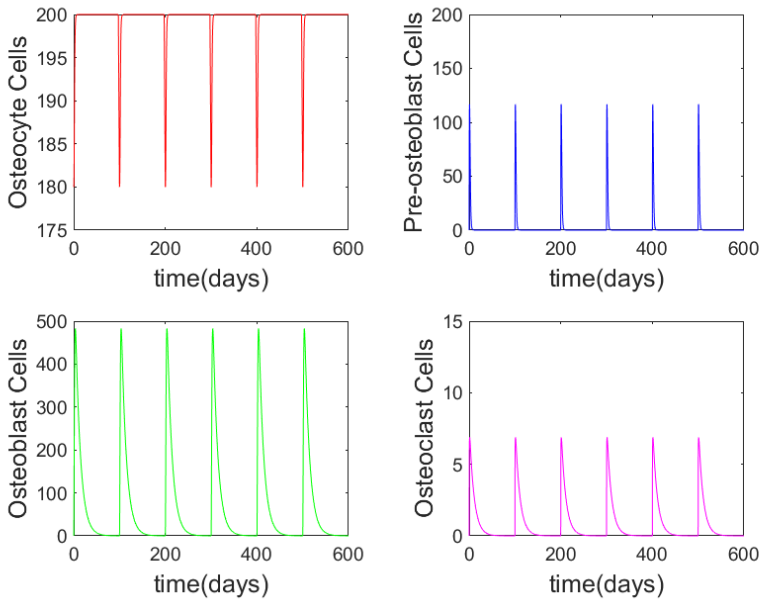

Figure 5.5: Activated cell population results for a normalized 50 fold increase in Wnt-10b: The cell dynamics do not deviate from the previous cases (Figures 5.3 and 5.4). The decrease in the maximum activated pre-osteoblasts and osteoclasts does become more significant than the previous case. The maximum activated osteoblast and osteocyte population continues to remain consistent throughout all three cases.

The activated pre-osteoblast cell population decreases with increasing Wnt-10b levels as well as the activated osteoclast population (Figures 5.6 and 5.7). Bennett et al. (2007) experimentally tested Wnt-10b causing a reduction in osteoclast population for mice with a normalized 5 fold increase in Wnt-10b, but found that the changes in mice osteoclasts on the perimeter of the bone not to be statistically significant (Figure 5.8). Our model does show that for a normalized 5 fold change in Wnt-10b the maximum activated osteoclast population changes less than two cells over one and a half remodeling cycles. For a normalized 50 fold change, our model predicts a much greater change in the maximum activated osteoclast cell population. The maximum activated osteoclast population reduces by six cells over one and a half remodeling cycles. That would be statistically significant. This correlation is more than likely due to a change in autocrine and paracrine signaling levels caused by the increase of Wnt-10b.

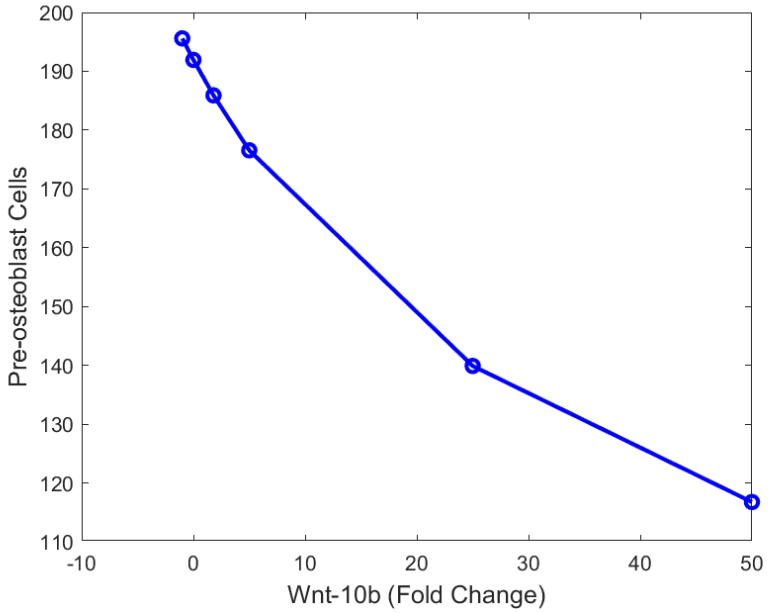

Figure 5.6: Pre-osteoblast cell population at varying levels of normalized Wnt-10b fold change: The maximum activated cell population of pre-osteoblasts was determined over a range of normalized Wnt-10b fold changes after running the simulation for one and a half remodeling cycles. The circles indicate the normalized fold changes that were input into the simulation. The simulation shows a negative correlation between maximum activated pre-osteoblast cell population and Wnt-10b.

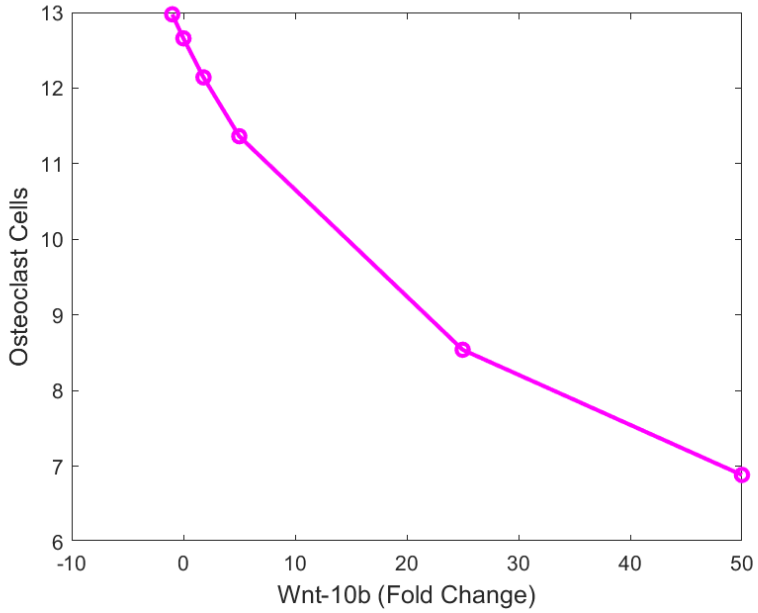

Figure 5.7: Osteoclast cell population at varying levels of Wnt-10b fold change: The maximum activated cell population of osteoclasts was determined over a range of normalized Wnt-10b fold changes after running the simulation for one and a half remodeling cycles. The circles indicate the normalized fold changes that were input into the simulation. The simulation shows a negative correlation between osteoclast cell population and Wnt-10b.

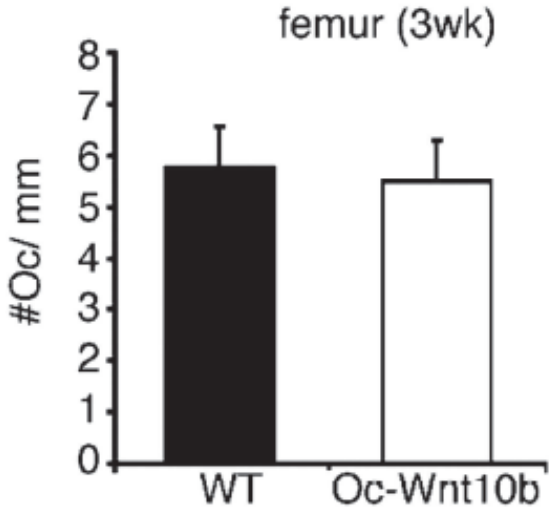

Figure 5.8: Osteoclast number on sections of femur for 3 week old mice (Bennett et al., 2007): The bar graph compares the number of osteoclasts per milimeter of bone for an unaltered (WT) mouse and a genetically altered (OC-Wnt10b) mouse. The OC-Wnt10b mouse has a normalized 5 fold increase of Wnt-10b over the WT mouse. At three weeks, or one and a half remodeling cycles, there is a slight decrease in OC-Wnt10b osteoclasts compared to WT osteoclasts. This decrease is not significant at a normalized 5 fold change, but it could indicate a negative correlation between osteoclast cell population and Wnt-10b at greater fold changes.

CHAPTER VI

Conclusion

6.1 Discussion

Understanding the relationship between bone metabolism and the immune system is a high priority to prevent osteoperosis. Though there are a few published models about bone metabolism, the model developed in this project provides new insight on how chronic changes in Wnt-10b can alter a bone remodeling cycle. As discussed in Chapter III, experimentally Wnt-10b as been shown to alter osteoblastogenesis, osteoblast apoptosis, and osteoblast bone formation rates. However, our simulation showed that these changes had little effect on the overall osteoblast population. Instead it seems as though the changes in these parameters might result in a population change of pre-osteoblast and osteoclasts. This could be due to the changes in autocrine and paracrine signaling. It could also be due to the fact that we did not independently model the effect of Wnt-10b on osteoblast formation, instead we kept the relationship coupled to the paracrine signaling of pre-osteoblasts and osteoclasts. Either way, these results could be the basis of a new experimental design that could provide a better understanding about this Wnt-10 and bone metabolism relationship.

Establishing a relationship between Wnt-10b and bone metabolism is a small step towards a better understanding of osteoimmunology. This model is especially interesting because it has already been shown experimentally that an immune response in the gut can induce T cells to secrete Wnt-10b (Tyagi et al., 2018). This provides us with information to combine this model with a mulitcompartment model of this response that has been developed in our lab.

6.2 Future Work

We are currently preparing this model for publication, but there are still modifications that need to be made before publication and other additions that we would like to make in the future. We would like to:

- Alter our model to be representative of a typical 200 day remodeling time period for humans (Jilka, 2013; Parfitt, 2002);
- Look at fitting the data point from Bennett et al. (2005) at twelve remodeling cycles since the measurements were taken from 6 month old mice;
- Explore the biological relevance of the predicted decrease in pre-osteoblast and osteoclasts
- Combine this model with a model that predicts how LGG induces an immune response that leads to an increase in Wnt-10b levels;
- Expand the model to include other biological chemicals of interest such as TNF-α (experimentally shown to alter osteoclast formation and activity), and IL-6 (experimentally shown to alter osteoclast formation) (Ponzetti and Rucci, 2019).

References

Araujo, A., Cook, L. M., Lynch, C. C., and Basanta, D. (2014). An integrated computational model of the bone microenvironment in bone-metastatic prostate cancer. *Cancer Res.*, 74(9):2391–2401.

Ayati, B. P., Edwards, C. M., Webb, G. F., and Wikswo, J. P. (2010). A mathematical model of bone remodeling dynamics for normal bone cell populations and myeloma bone disease. *Biol. Direct*, 5(1):28.

Bennett, C. N., Longo, K. A., Wright, W. S., Suva, L. J., Lane, T. F., Hankenson, K. D., and MacDougald, O. A. (2005). Regulation of osteoblastogenesis and bone mass by Wnt-10b. *Proc. Natl. Acad. Sci. U. S. A.*, 102(9):3324–3329.

Bennett, C. N., Ouyang, H., Ma, Y. L., Zeng, Q., Gerin, I., Sousa, K. M., Lane, T. F., Krishnan, V., Hankenson, K. D., and MacDougald, O. A. (2007). Wnt-10b increases postnatal bone formation by enhancing osteoblast differentiation. *J. Bone Miner. Res.*, 22(12):1924–1932.

Bucher, C. H., Schlundt, C., Wulsten, D., Sass, F. A., Wendler, S., Ellinghaus, A., Thiele, T., Seemann, R., Willie, B. M., Volk, H.-D., et al. (2019). Experience in the adaptive immunity impacts bone homeostasis, remodeling, and healing. *Front. Immunol.*, 10:797.

Chang, Y., Cho, B., Kim, S., and Kim, J. (2019). Direct conversion of fibroblasts to osteoblasts as a novel strategy for bone regeneration in elderly individuals. *Exp. Mol. Med.*, 51(5):1–8.

Cook, L. M., Araujo, A., Pow-Sang, J. M., Budzevich, M. M., Basanta, D., and Lynch, C. C. (2016). Predictive computational modeling to define effective treatment strategies for bone metastatic prostate cancer. *Sci. Rep.*, 6:29384.

Croes, M., Kruyt, M., Loozen, L., Kragten, A., Yuan, H., Dhert, W., Öner, F., and Alblas, J. (2017). Local induction of inflammation affects bone formation. *Eur. Cells Mater.*, 33:211–226.

Eriksen, E. F. (2010). Cellular mechanisms of bone remodeling. *Rev. Endocr. Metab. Disord.*, 11(4):219–227.

Graham, J., Ayati, B., Holstein, S., and Martin, J. (2013). The role of osteocytes in targeted bone remodeling: a mathematical model. *PLoS ONE*, 8(5).

Harvey, N., Dennison, E., and Cooper, C. (2010). Osteoporosis: impact on health and economics. *Nat. Rev. Rheumatol.*, 6(2):99.

Jamali, Z., Arababadi, M. K., and Asadikaram, G. (2013). Serum levels of IL-6, IL-10, IL-12, IL-17 and IFN-γ and their association with markers of bone metabolism in vitamin D-deficient female students. *Inflammation*, 36(1):164–168.

Jilka, R. L. (2013). The relevance of mouse models for investigating age-related bone loss in humans. *J Gerontol A Biol Sci Med Sci.*, 68(10):1209–1217.

Jing, H., Su, X., Gao, B., Shuai, Y., Chen, J., Deng, Z., Liao, L., and Jin, Y. (2018). Epigenetic inhibition of Wnt pathway suppresses osteogenic differentiation of BMSCs during osteoporosis. *Cell Death Dis.*, 9(2):1–12.

Kato, M., Patel, M. S., Levasseur, R., Lobov, I., Chang, B. H.-J., Glass, D. A., Hartmann, C., Li, L., Hwang, T.-H., Brayton, C. F., et al. (2002). Cbfa1-independent decrease in osteoblast proliferation, osteopenia, and persistent embryonic eye vascularization in mice deficient in Lrp5, a Wnt coreceptor. *JCB*, 157(2):303–314.

Komarova, S. V. (2005). Mathematical model of paracrine interactions between osteoclasts and osteoblasts predicts anabolic action of parathyroid hormone on bone. *Endocrinology*, 146(8):3589–3595.

Komarova, S. V., Safranek, L., Gopalakrishnan, J., Ou, M.-j. Y., McKee, M. D., Murshed, M., Rauch, F., and Zuhr, E. (2015). Mathematical model for bone mineralization. *Front. Cell Dev. Biol.*, 3:51.

Komarova, S. V., Smith, R. J., Dixon, S. J., Sims, S. M., and Wahl, L. M. (2003). Mathematical model predicts a critical role for osteoclast autocrine regulation in the control of bone remodeling. *Bone*, 33(2):206–215.

Leibbrandt, A. and Penninger, J. M. (2008). RANK/RANKL: regulators of immune responses and bone physiology. *Ann. N. Y. Acad. Sci.*, 1143(1):123–150.

Longo, K. A., Wright, W. S., Kang, S., Gerin, I., Chiang, S.-H., Lucas, P. C., Opp, M. R., and MacDougald, O. A. (2004). Wnt-10b inhibits development of white and brown adipose tissues. *J. Biol. Chem.*, 279(34):35503–35509.

Madel, M.-B., Ibáñez, L., Wakkach, A., De Vries, T. J., Teti, A., Apparailly, F., and Blin-Wakkach, C. (2019). Immune function and diversity of osteoclasts in normal and pathological conditions. *Front. Immunol.*, 10:1408.

Nanjundaiah, S., Stains, J., and Moudgil, K. (2013). Kinetics and interplay of mediators of inflammation-induced bone damage in the course of adjuvant arthritis. *Int. J. Immunopathol. Pharmacol.*, 26(1):37–48.

Pacifici, R. (2013). Role of T cells in the modulation of PTH action: physiological and clinical significance. *Endocrine*, 44(3):576–582.

Parfitt, A. (2002). Targeted and nontargeted bone remodeling: relationship to basic multicellular unit origination and progression. *Bone*, 30(1):5–7.

Parfitt, A. M. (1994). Osteonal and hemi-osteonal remodeling: the spatial and temporal framework for signal traffic in adult human bone. *J. Cell. Biochem.*, 55(3):273–286.

Patsch, J. M., Kohler, T., Berzlanovich, A., Muschitz, C., Bieglmayr, C., Roschger, P., Resch, H., and Pietschmann, P. (2011). Trabecular bone microstructure and local gene expression in iliac crest biopsies of men with idiopathic osteoporosis. *J. Bone Miner. Res.*, 26(7):1584–1592.

Peterson, M. C. and Riggs, M. M. (2010). A physiologically based mathematical model of integrated calcium homeostasis and bone remodeling. *Bone*, 46(1):49–63.

Ponzetti, M. and Rucci, N. (2019). Updates on osteoimmunology: what's new on the cross-talk between bone and immune system. *Front. Endocrinol.*, 10:236.

Raggatt, L. J. and Partridge, N. C. (2010). Cellular and molecular mechanisms of bone remodeling. *J. Biol. Chem.*, 285(33):25103–25108.

Rattanakul, C., Lenbury, Y., Krishnamara, N., and Wollkind, D. J. (2003). Modeling of bone formation and resorption mediated by parathyroid hormone: response to estrogen/PTH therapy. *BioSystems*, 70(1):55–72.

Roser-Page, S., Vikulina, T., Zayzafoon, M., and Weitzmann, M. N. (2014). Ctla-4ig-induced T cell anergy promotes Wnt-10b production and bone formation in a mouse model. *Arthritis Rheumatol.*, 66(4):990–999.

Targońska, M., Kochanowska, I., Ostrowski, K., and Gorski, A. (2001). Osteoimmunology: new area of research on the associations between the immune and bone systems. *Pol. Arch. Med. Wewn.*, 105(5):435.

Theill, L. E., Boyle, W. J., and Penninger, J. M. (2002). RANKL and RANK: T cells, bone loss, and mammalian evolution. *Annu. Rev. Immunol.*, 20(1):795–823.

Tyagi, A. M., Yu, M., Darby, T. M., Vaccaro, C., Li, J.-Y., Owens, J. A., Hsu, E., Adams, J., Weitzmann, M. N., Jones, R. M., et al. (2018). The microbial metabolite butyrate stimulates bone formation via T regulatory cell-mediated regulation of Wnt-10b expression. *Immunity*, 49(6):1116–1131.

Walker-Bone, K. (2012). Recognizing and treating secondary osteoporosis. *Nat. Rev. Rheumatol.*, 8(8):480.

Walsh, M. C., Kim, N., Kadono, Y., Rho, J., Lee, S. Y., Lorenzo, J., and Choi, Y. (2006). Osteoimmunology: interplay between the immune system and bone metabolism. *Annu. Rev. Immunol.*, 24:33–63.

Wend, P., Wend, K., Krum, S., and Miranda-Carboni, G. (2012). The role of Wnt-10b in physiology and disease. *Acta Physiol.*, 204(1):34–51.

Xiao, L., Zhou, Y., Zhu, L., Yang, S., Huang, R., Shi, W., Peng, B., and Xiao, Y. (2018). SPHK1-S1PR1-RANKL axis regulates the interactions between macrophages and bmscs in inflammatory bone loss. *J. Bone Miner. Res.*, 33(6):1090–1104.

Xie, Y., Zhang, L., Xiong, Q., Gao, Y., Ge, W., and Tang, P. (2019). Bench-to-bedside strategies for osteoporotic fracture: from osteoimmunology to mechanosensation. *Bone Res.*, 7(1):1–13.

Yang, Y., Wang, X., Miron, R. J., and Zhang, X. (2019). The interactions of dendritic cells with osteoblasts on titanium surfaces: an in vitro investigation. *Clin. Oral Investig.*, 23(11):4133–4143.

APPENDIX A

Data Images

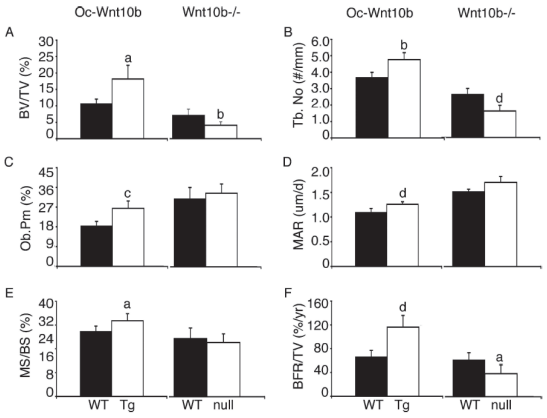

FIG. 4. Bone formation rates in Oc-Wnt10b and Wnt10b$^{-/-}$ mice. Mineralization of bone was evaluated with calcein labeling in Oc-Wnt10b (Tg), Wnt10b$^{-/-}$ (null), and littermate controls (WT) mice at 3 mo of age. Femurs were isolated and sectioned for static and dynamic histomorphometry. (A) Bone volume/total volume (BV/TV; %), (B) trabecular number (Tb.No.; #/mm), (C) osteoblast perimeter (Ob.Pm.; %), (D) mineral apposition rate (MAR; μm/d), (E) mineralizing surface/bone surface (MS/BS; %), and (F) bone formation rate/tissue volume (BFR/TV; %/yr) are presented as mean ± SE. $^{a}p < 0.05$, $^{b}p < 0.01$, $^{c}p < 0.005$, $^{d}p < 0.001$ ($n = 6$).

Figure A.1: Graphs provided in Bennett et al. (2007) used for model parameterization

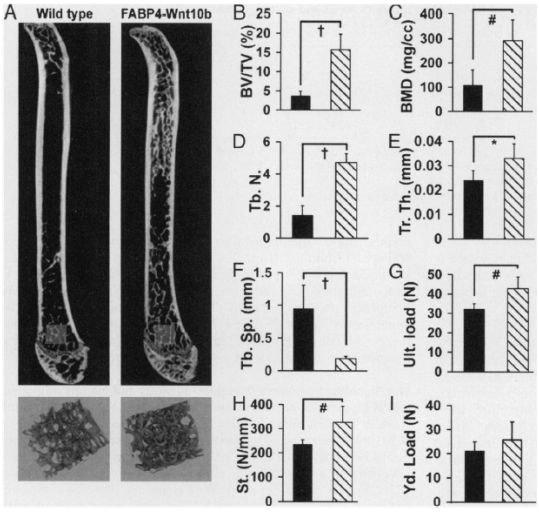

Fig. 1. Increased bone mass and strength in FABP4-Wnt10b mice. (*A*) μCT of femurs from wild-type and FABP4-Wnt10b mice (*Upper*). Three-dimensional reconstructions of metaphyseal trabeculae from regions highlighted (*Lower*). Morphometric properties of 1 mm^3 of distal femur from wild-type (■) and FABP4-Wnt10b (▨) mice at 6 months of age were analyzed for bone volume fraction (*B*; BV/TV, %), bone mineral density (*C*; BMD), trabecular number (*D*; Tr. N.), trabecular thickness (*E*; Tb. Th.), trabecular spacing (*F*; Tb. Sp.), ultimate load (*G*), stiffness (*H*), and yield load (*I*). Statistical significance for each measurement was evaluated with Student's *t* test: $P < 0.05$ (•), < 0.01 (#), < 0.001 (†), with $n = 6$ males for each genotype.

Figure A.2: Graphs provided in Bennett et al. (2005) used for model parameterization

Table 1. Micro-CT–assessed bone structure indices in the L3 vertebrae and femora of young mice administered Ig (control) or CTLA-4Ig for 3 months or 6 months*

Treatment duration, site, index	Ig	CTLA-4Ig	% change	*P*
3 months				
L3 vertebra				
BV/TV, %	13.15 ± 1.25	15.07 ± 0.95	14.6	0.0011
TbTh, mm	0.0390 ± 0.0010	0.0406 ± 0.0024	4.0	0.0761
TbN, mm	3.71 ± 0.20	3.91 ± 0.24	5.4	0.0566
TbSp, mm	0.2675 ± 0.0147	0.2526 ± 0.0161	−5.6	0.0439
Femur				
BV/TV, %	6.35 ± 1.35	8.04 ± 1.22	18.8	0.0088
TbTh, mm	0.0412 ± 0.0026	0.0433 ± 0.0037	4.9	0.1490
TbN, /mm	3.44 ± 0.34	3.69 ± 0.32	−0.4	0.1091
TbSp, mm	0.2822 ± 0.0147	0.2713 ± 0.0247	2.0	0.2451
CoAr, mm^2	0.8074 ± 0.0322	0.8068 ± 0.0339	−0.1	0.9696
CoTh, mm	0.1840 ± 0.0054	0.1864 ± 0.0065	1.3	0.3830
6 months				
L3 vertebra				
BV/TV, %	13.33 ± 1.05	16.91 ± 1.76	26.9	<0.0001
TbTh, mm	0.0450 ± 0.0027	0.0474 ± 0.0026	5.3	0.0447
TbN, /mm	3.15 ± 0.12	3.53 ± 0.31	12.1	<0.0001
TbSp, mm	0.3195 ± 0.0155	0.2843 ± 0.0222	−11.0	0.0002
Femur				
BV/TV, %	3.24 ± 1.01	4.42 ± 1.32	36.6	0.0262
TbTh, mm	0.0442 ± 0.0045	0.0485 ± 0.0060	9.7	0.0631
TbN, /mm	2.67 ± 0.19	2.76 ± 0.16	3.4	0.2349
TbSp, mm	0.3791 ± 0.0273	0.3666 ± 0.0243	−3.3	0.2640
CoAr, mm^2	0.7462 ± 0.0268	0.7835 ± 0.0597	5.0	0.0630
CoTh, mm	0.1898 ± 0.0072	0.2000 ± 0.0104	5.4	0.0114

* Values are the mean ± SD (n = 10, 3-month Ig treatment and 3-month CTLA-4Ig treatment; n = 12, 6-month Ig treatment; n = 11, 6-month CTLA-4Ig treatment). Micro-CT = micro–computed tomography; BV/TV = bone volume/total volume; TbTh = trabecular thickness; TbN = trabecular number; TbSp = trabecular separation; CoAr = cortical area; CoTh = cortical thickness.

Figure A.3: BV/TV values for 1.8 Wnt-10b fold increase used for model validation (Roser-Page et al., 2014)

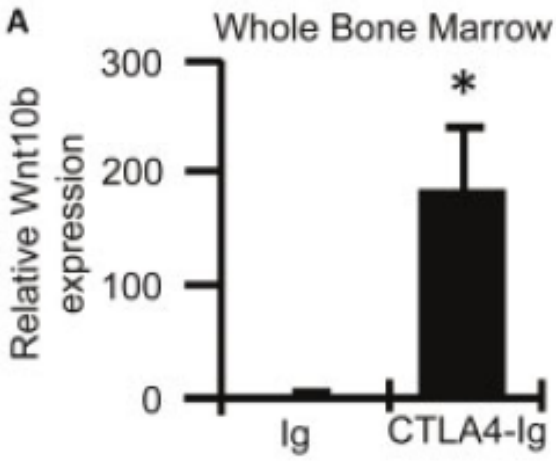

Figure A.4: Wnt-10b relative expression for data from Roser-Page et al. (2014) used for model validation

APPENDIX B

MATLAB Code

Parameter Estimation Code

```
%Carley Cook
% This code was written to estimate the change in parameters when ...
    a change
% in Wnt10b occurs
%% Data from Bennett 2005 and Bennett 2007
clear
close all
format long e
xdata=[-1, 5, 50]; %Wnt10b Fold Change
ydata=[-29.7,  69.2, 339]; % Bennet Data normalized BV/TV %.339 I ...
    ommited one set of OC data is because it is a repeated data point

ParamY=2;% ParamY=1 for running parameter estimation code
         % ParamY=2 for just graphing
K2type=2;%LinearK2=1 linear with wnt10b
            %LinearK2=2 MM with wnt10b
kM=25; %kM for MM with k2 Try 50 or 25
N=1; %Number of Cylces
cyclelength=100; %length of cylces
tlag=14; %DDE lag from osteoblast maturation to activation
Gwntdose=0; %Dose of wnt that will be graphed
%% Guesses for the parameters

kg(1)= 5e-03 ;%beta1adj
              %For Linear:5.873531975374805e-03 ...
                 resnorm:1.449131332295683e+02
              %For kM 25:5.018040516139597e-03 ...
                 resnorm:1.540881900659893e+02
                %Rounding to 5 sig figs does not alter resnorm ...
                   for kM=25
                %Rounding as shown below alters only slightly ...
                   assume same
                %resnorm
                %5e-03
              %For kM 50:5.510605529240327e-03 ...
                 resnorm:1.513236172705052e+02
kg(2)=1.5e-04;%beta2adj
              %For Linear:1.499999999763948e-04
```

```
32                %1.499999999729445e-04 This value is the actual ...
                     number given
33                %by param estimation
34                %1.5e-04
35 kg(3)=1.6828e-03;%k2adj
36               %For Linear:1.517244270770526e-05
37               %For kM 25:1.682813357447710e-03
38                  %1.6828e-03
39               %For kM 50:1.807770227757210e-03
40 kguess=kg;
41
42 %Setting guesses to k values if only graphing
43 if ParamY==2
44     k=kg;
45 end
46
47
48 %% Initial conditions
49 % S0=200 for SS and K_S-rho=(180) for activation
50 S0=180; % Initial Osteocytes
51 P0=0; %Initial Pre-Osteoblasts
52 B0=0; %Initial Osteoblasts
53 C0=0; %Initial Osteoclasts
54 z0=100; %Initial Bone Volume
55 y0=[S0,P0,B0,C0,z0]; % Initial conditions in vector
56
57 %% Parameter Estimation with k parameters, BV, and resnorm outputs
58 %Turning on parameter estimation
59 if ParamY==1
60 OPTIONS = optimoptions('lsqcurvefit','StepTolerance',1e-16,...
61     'FunctionTolerance',1e-16,'optimalitytolerance', 1e-16);
62 lb=[-0.1/50,-0.1,0];
63 %lb=[0,0,0];
64 %ub=[0.1,0.1/50,Inf];
65 ub=[Inf,0.00015,Inf];
66 %[k,resnorm] = lsqcurvefit(@(k,xdata) ...
      Graham2013(k,xdata,y0,N,cyclelength,tlag),kguess,xdata,ydata, ...
      lb, ub)%, OPTIONS)
67 [k,resnorm,residual] = lsqcurvefit(@(k,xdata) ...
      Graham2013(k,xdata,y0,...
68     N,cyclelength,tlag,kM,K2type),kguess,xdata,ydata, lb, ub, ...
           OPTIONS)
69 %% Final k values beta1adj and beta2adj
70        k1f=k(1) %beta1adj
71        k2f=k(2) %beta2adj
72        k3f=k(3) %k2adj
73 end
74 %% Graphing of BV vs Wnt
75 figure(1)
76  %xp = linspace(xdata(1),xdata(end),1001);
77  %xp = linspace(xdata(1),xdata(end),100);
78  xp = linspace(-1,50,100);
79  ycalcp = Graham2013(k,xp,y0,N,cyclelength,tlag,kM,K2type);
80  plot(xp,ycalcp(1,:),'r','Linewidth',2);
```

```
 hold on
 plot(xdata,ydata,'o')
legend("Simulation Results","Literature ...
    Data",'Location','Best','FontSize',12)
xlabel('Wnt-10b (Fold Change)','FontSize',15)
ylabel('BV//TV (% Change from normal Wnt-10b)','FontSize',15)


%Plot all cases on the same graph

%% Graphing of Cells and Bone Volume vs time
figure(2)
[tcalcpt,ycalcpt]=Cyclefunction(k,Gwntdose,y0,N,cyclelength,tlag,...
    kM,K2type);

tiledlayout(2,2)
%Osteocytes
nexttile
plot(tcalcpt,ycalcpt(:,1),'r-');
xlabel('time(days)')
ylabel('Osteocyte Cells')

%Pre-osteoblasts
nexttile
plot(tcalcpt,ycalcpt(:,2),'b-');
xlabel('time(days)')
ylabel('Pre-osteoblast Cells')

%Osteoblasts
nexttile
plot(tcalcpt,ycalcpt(:,3),'g-');
xlabel('time(days)')
ylabel('Osteoblast Cells')

%Osteoclasts
nexttile
plot(tcalcpt,ycalcpt(:,4),'m-');
xlabel('time(days)')
ylabel('Osteoclast Cells')

figure(3)
plot(tcalcpt,ycalcpt(:,5),'g-','Linewidth',2)
xlabel('time(days)','FontSize',15)
ylabel('Relative bone volume (%)','FontSize',15)




%% History functions for the DDE
function historyV1 =history1(t,y0,k,xdata,oldsol,kM,K2type)

historyV1=y0'; % Initial conditions in vector
if t<0
    historyV1(1)=200;
```

```
134 else
135     historyV1(1)=180;
136 end
137
138
139 end
140 function historyV2 =history2(t,y0,k,xdata,oldsol,kM,K2type)
141
142 historyV2=deval(oldsol,t); % Initial conditions in vector
143 %Refers to function that already resets for next time interval
144 % if t<0
145 %     historyV2(1)=200;
146 % else
147 %     historyV2(1)=180;
148 % end
149
150
151 end
152 %% Define ODE equations with variable parameters
153 function dydt= ddefun(t,y,Z,y0,k,x,oldsol,kM,K2type)%x is a ...
       scalar wnt10b dose
154
155 Bone=1;
156 alpha_1=0.5;
157 alpha_2=0.1;
158 alpha_3=0.1;
159 beta_1=0.1;
160 delta=0.1;
161 beta_2=0.1;
162 alpha_4=0.1;
163 K_S=200;
164 k1=.69825;%Graham2013 paper has .7 to get the ss to 100 .6983 ...
       works for ode
165           %When dde .69825
166           %When dde with round(c).71575
167           %When dde with round(c) in dcdt .72249
168 k2=0.015445;
169 g_31=1;
170 g_21=2;
171 g_22=1;
172 g_32=1;
173 g_41=1;
174 g_42=1;
175 g_43=-1;
176 g_44=1;
177 f_12=1;
178 f_14=1;
179 f_23=1;
180 f_34=1;
181 epsilon=1;
182 beta_3=0.1;
183 rho=20;
184
185     S =y(1);
```

```
186     P =y(2);
187     B =y(3);
188     C =y(4);
189     z=y(5);
190     ylag=Z(:,1);
191     Blag=ylag(3);
192
193
194     %Set parameter definitions
195     beta1adj = k(1);
196     beta2adj = k(2);
197     k2adj=k(3);
198
199     %Setting k2 relationship to wnt
200     if K2type==1
201        knew=k2+(k2adj*x);
202     elseif K2type==2
203        knew=k2+((k2adj*x)/(x+kM));
204     end
205
206     %Algebraic equations needed for the ODEs
207     Differentiation_of_Osteoblast_to_Osteocytes = ...
           Bone*alpha_1*power(B,g_31)*max((1-S/K_S),0);
208     Differentiation_of_MSC_cells_to_PreOsteoblast_cells = ...
           Bone*alpha_2*power(S,g_21)*max((1-S/K_S),0)^g_22;
209     Proliferation_of_preosteoblasts = ...
           Bone*alpha_3*power(P,g_32)*max((1-S/K_S),0);
210     Differentiation_of_PreOsteoblast_to_mature_osteoblast = ...
           Bone*(beta_1+(beta1adj*x))*power(P,f_12)*power(C,f_14);
211     %Differentiation_of_PreOsteoblast_to_mature_osteoblast = ...
           Bone*(beta_1+(beta1adj*x))*power(P,f_12)*power(round(C),f_14);
212     Apoptosis_of_preosteoblast = Bone*delta*P;
213     Apoptosis_of_osteoblasts = ...
           Bone*(beta_2-(beta2adj*x))*power(B,f_23);
214     Differentiation_of_preosteoclast_to_osteoclasts = ...
           Bone*alpha_4*power...
215         (S,g_41)*power(P,g_42)*power(epsilon+B,g_43)*...
216         max((1-S/K_S),0)^g_44;
217     Apoptosis_of_osteoclasts = Bone*beta_3*power(C,f_34);
218     %Apoptosis_of_osteoclasts = Bone*beta_3*power(round(C),f_34);
219     Resorption_of_bone = Bone*k1*C;
220     %Resorption_of_bone = Bone*k1*round(C);
221     Formation_of_bone = Bone*((knew*Blag));
222     %Formation_of_bone = Bone*((knew*B));
223     %ODEs
224
225     %d([Osteocytes (S)])/dt = ...
           1/Bone*Differentiation_of_Osteoblast_to_Osteocytes;
226     dydt(1)=1/Bone*Differentiation_of_Osteoblast_to_Osteocytes;
227
228     %d([Pre-Osteoblasts (P)])/dt = ...
           1/Bone*(Differentiation_of_MSC_cells_to_PreOsteoblast_cells ...
           + Proliferation_of_preosteoblasts - ...
           Differentiation_of_PreOsteoblast_to_mature_osteoblast - ...
```

```
        Apoptosis_of_preosteoblast)
229     dydt(2)=1/Bone*...
230         (Differentiation_of_MSC_cells_to_PreOsteoblast_cells ...
231         + Proliferation_of_preosteoblasts - ...
232         Differentiation_of_PreOsteoblast_to_mature_osteoblast...
233         - Apoptosis_of_preosteoblast);
234
235     %d([Osteoblasts (B)])/dt = 1/Bone*
236     %(-Differentiation_of_Osteoblast_to_Osteocytes +
237     %Differentiation_of_PreOsteoblast_to_mature_osteoblast
238     %- Apoptosis_of_osteoblasts)
239     dydt(3)=1/Bone*(-Differentiation_of_Osteoblast_to_Osteocytes...
240         + Differentiation_of_PreOsteoblast_to_mature_osteoblast...
241         - Apoptosis_of_osteoblasts);
242
243     %d([Osteoclasts (C)])/dt = ...
        1/Bone*(Differentiation_of_preosteoclast_to_osteoclasts - ...
        Apoptosis_of_osteoclasts)
244     dydt(4)=1/Bone*(Differentiation_of_preosteoclast_to_osteoclasts...
245         - Apoptosis_of_osteoclasts);
246
247     %d([Bone volume (z)])/dt = 1/Bone*(-Resorption_of_bone + ...
        Formation_of_bone)
248     dydt(5)=1/Bone*(-Resorption_of_bone + Formation_of_bone);
249
250
251     dydt=[dydt(1)
252           dydt(2)
253           dydt(3)
254           dydt(4)
255           dydt(5)];
256
257 end
258
259 %% Solve ODE using variable parameters
260 function yout = Graham2013(k,xdata,y0,N,cyclelength,tlag,kM,K2type)
261
262     for i = 1:length(xdata)
263
264         [~,ycalc] = ...
              Cyclefunction(k,xdata(i),y0,N,cyclelength,tlag,kM,K2type);
265
266         yBV(i,1)=ycalc(end,5);
267         yout(i,1)=yBV(i,:)-100;
268
269
270     end
271     yout = yout';
272 end
273 %% Cycle Function
274      function [combined_tcalc_N_cycles, combined_ycalc_N_cycles] ...
           = Cyclefunction(k,xdata,y0,N,cyclelength,tlag,kM,K2type)
275      startindex=1; %Indices are used to combine the loops into a ...
           single column
```

```
276       finalindex=1;
277       oldsol=[];
278            for j= 1:N
279
280              %tspan = (j-1)*cyclelength:0.01:j*cyclelength;
281              %tspan =linspace((j-1)*cyclelength,j*cyclelength,101);
282              tspan = [(j-1)*cyclelength,j*cyclelength];
283               %[tcalc,ycalc] = ode23s(@(t,y) ...
                     ODEeq(t,y,k,xdata(i)),tspan,y0);
284               %[tcalc,ycalc] = ode23s(@(t,y) ...
                     ODEeq(t,y,k,xdata),tspan,y0);
285               %sol = dde23(@(t,y) ...
                     ddefun(t,y,Z,k,xdata),[14],@history,tspan,y0);
286
287               if j==1
288                  %Uses initial condition vector as history
289                  sol = dde23(@ddefun,tlag,@history1,...
290                      tspan,[],y0,k,xdata,oldsol,kM,K2type);
291                  oldsol=sol; %saves solution as a history solution
292               else
293                  %Uses history solution as history function
294                  sol = dde23(@ddefun,tlag,@history2,...
295                      tspan,[],y0,k,xdata,oldsol,kM,K2type);
296                  oldsol=sol; %saves solution as a history solution
297               end
298               tcalc=sol.x';
299               ycalc=sol.y';
300               ycalc(:,1);
301               %Reset for next time interval
302               y0=ycalc(end,:);
303               idx=(y0<1);
304               y0(idx)=0; %Sets fractions of cells to zero
305               y0(1,1)=y0(1,1)-20; %Reduces osteocytes to initate ...
                     next cycle
306               oldsol.y(:,end)=y0';
307               finalindex=finalindex+length(tcalc)-1;
308               combined_tcalc_N_cycles(startindex:finalindex,1)=tcalc;
309               combined_ycalc_N_cycles(startindex:finalindex,:)=ycalc;
310               startindex=startindex+length(tcalc)-1; %equals ...
                     previous final index
311            end
312
313       end
```

Graphing Code

```
1  %Carley Cook
2  % This code was written to produce graphs for the Wnt-10b and ...
       bone volume
3  % project
4  %% Data from Bennett 2005 and Bennett 2007
```

```
clear
close all
format long e
xdata=[-1, 5, 50]; %Wnt10b Fold Change
ydata=[-29.7,  69.2, 339]; % Bennet Data normalized BV/TV

kM=25; %kM for MM with k2 Try 50 or 25
N=6; %Number of Cylces
cyclelength=100; %length of cylces
tlag=14; %DDE lag from osteoblast maturation to activation
savegraphs=2; %1 for automatically saving graphs
              %2 for manual saving of graphs
BVandCells=2;%1 to produce Bone Volume and cells for each graph
Estimationcase=2; %1 to produce estimation cases on same graph
Validationcase=2; %1 to produce validation case
OCWnt=1; %1 to produce cells vs wnt
barg=2; %1 to produce a bar graph of Wnt fold changes
%% Fitted parameters
kg(1)= 5e-03 ;%beta1adj

kg(2)=1.5e-04;%beta2adj

kg(3)=1.6828e-03;%k2adj

k=kg;

%% Initial conditions
S0=180; % Initial Osteocytes
P0=0; %Initial Pre-Osteoblasts
B0=0; %Initial Osteoblasts
C0=0; %Initial Osteoclasts
z0=100; %Initial Bone Volume
y0=[S0,P0,B0,C0,z0]; % Initial conditions in vector

%% Graphing of Cells and Bone Volume vs time for all cases
if BVandCells==1
    Gwntdose= [-1 0 1.8 1.8 5 50]; %Dose of wnt that will be graphed
    for i=1:length(Gwntdose)
        l='FoldChangeCells';
        l2='FoldChangeBone';
        N=6;
        if i==4
            N=12;
        end


    [tcalcpt,ycalcpt]=Cyclefunction(k,Gwntdose(i),y0,N,...
        cyclelength,tlag,kM);

    %Cells
        figure(i)
        tiledlayout(2,2)
        %Osteocytes
        nexttile
```

```
59          plot(tcalcpt,ycalcpt(:,1),'r-');
60          xlabel('time(days)','FontSize',12)
61          ylabel('Osteocyte Cells','FontSize',12)
62
63          %Pre-osteoblasts
64          nexttile
65          plot(tcalcpt,ycalcpt(:,2),'b-');
66          axis([0 N*100 0 200])
67          xlabel('time(days)','FontSize',12)
68          ylabel('Pre-osteoblast Cells','FontSize',12)
69
70          %Osteoblasts
71          nexttile
72          plot(tcalcpt,ycalcpt(:,3),'g-');
73          xlabel('time(days)','FontSize',12)
74          ylabel('Osteoblast Cells','FontSize',12)
75
76          %Osteoclasts
77          nexttile
78          plot(tcalcpt,ycalcpt(:,4),'m-');
79          axis([0 N*100 0 15])
80          xlabel('time(days)','FontSize',12)
81          ylabel('Osteoclast Cells','FontSize',12)
82
83      %Bone Volume
84          figure(i+6)
85          plot(tcalcpt,ycalcpt(:,5),'g-','Linewidth',2)
86          xlabel('time(days)','FontSize',12)
87          ylabel('Relative bone volume (%)','FontSize',12)
88
89
90      if savegraphs==1
91      q=string(Gwntdose(i));
92      v=strcat(l,q);
93      v2=strcat(l2,q);
94      if i== 3
95          q='18';
96          v=strcat(l,q);
97          v2=strcat(l2,q);
98      end
99      if i== 4
100         q='18';
101         w='12months';
102         v=strcat(l,q,w);
103         v2=strcat(l2,q,w);
104     end
105     saveas(figure(i),v,'png')
106     saveas(figure(i+6),v2,'png')
107     end
108
109     end
110 end
111 %% Graphing of cases used for parameter estimation
112 if Estimationcase==1
```

```
113     [tcalcpt1,ycalcpt1]=Cyclefunction(k,-1,y0,N,cyclelength,tlag,kM);
114     [tcalcpt5,ycalcpt5]=Cyclefunction(k,5,y0,N,cyclelength,tlag,kM);
115     [tcalcpt50,ycalcpt50]=Cyclefunction(k,50,y0,N,cyclelength,...
116         tlag,kM);
117         figure(13)
118         plot(tcalcpt1,ycalcpt1(:,5),'g-','Linewidth',2)
119         hold on
120         plot(tcalcpt5,ycalcpt5(:,5),'b:','Linewidth',2)
121         plot(tcalcpt50,ycalcpt50(:,5),'r-.','Linewidth',2)
122         plot(600,ydata+100,'ko','Linewidth',2)
123         legend("-1 Fold","5 Fold","50 Fold","Literature Data",...
124             'Location','Best','FontSize',12)
125         xlabel('time(days)','FontSize',15)
126         ylabel('Relative bone volume (%)','FontSize',15)
127
128     if savegraphs==1
129     saveas(figure(13),'EstimationResults','png')
130     end
131 end
132
133 %% Graphing of model validation
134 if Validationcase==1
135     [tcalcpt12,ycalcpt12]=Cyclefunction(k,1.8,y0,12,cyclelength,...
136         tlag,kM);
137     figure(14)
138         plot(tcalcpt12,ycalcpt12(:,5),'Linewidth',2)
139         hold on
140         errorbar( 600 , 126.6 , 15,'o','Linewidth',2 )
141         errorbar( 1200 , 136.6 , 29,'s','Linewidth',2 )
142         legend("Simulation Results","Data corresponding to 6 ...
                cylces",...
143              "Data corresponding to 12 cycles",'Location',...
144              'Best','FontSize',12)
145         xlabel('time(days)','FontSize',15)
146         ylabel('Relative bone volume (%)','FontSize',15)
147     if savegraphs==1
148     saveas(figure(14),'ValidationResults','png')
149     end
150 end
151
152 %% Graphing important cell population vs Wnt
153 if OCWnt==1
154     N=1.5;
155     [tcalcpt1,ycalcpt1]=Cyclefunction(k,-1,y0,N,...
156         cyclelength,tlag,kM);
157     [tcalcpt0,ycalcpt0]=Cyclefunction(k,0,y0,N,...
158         cyclelength,tlag,kM);
159     [tcalcpt18,ycalcpt18]=Cyclefunction(k,1.8,y0,N,...
160         cyclelength,tlag,kM);
161     [tcalcpt5,ycalcpt5]=Cyclefunction(k,5,y0,N,...
162         cyclelength,tlag,kM);
163     [tcalcpt25,ycalcpt25]=Cyclefunction(k,25,y0,N,...
164         cyclelength,tlag,kM);
165     [tcalcpt50,ycalcpt50]=Cyclefunction(k,50,y0,N,...
```

```
        cyclelength,tlag,kM);
    Gwntdose= [-1 0 1.8 5 25 50];
    figure(15)
        oc(1)=max(ycalcpt1(:,4));
        oc(2)=max(ycalcpt0(:,4));
        oc(3)=max(ycalcpt18(:,4));
        oc(4)=max(ycalcpt5(:,4));
        oc(5)=max(ycalcpt25(:,4));
        oc(6)=max(ycalcpt50(:,4));
        plot(Gwntdose,oc,'m-o','Linewidth',2);
        xlabel('Wnt-10b (Fold Change)','FontSize',12)
        ylabel('Osteoclast Cells','FontSize',12)

    figure(16)
        PO(1)=max(ycalcpt1(:,2));
        PO(2)=max(ycalcpt0(:,2));
        PO(3)=max(ycalcpt18(:,2));
        PO(4)=max(ycalcpt5(:,2));
        PO(5)=max(ycalcpt25(:,2));
        PO(6)=max(ycalcpt50(:,2));
        plot(Gwntdose,PO,'b-o','Linewidth',2);
        xlabel('Wnt-10b (Fold Change)','FontSize',12)
        ylabel('Pre-osteoblast Cells','FontSize',12)


    if savegraphs==1
    saveas(figure(15),'OCWnt','png')
    saveas(figure(16),'POWnt','png')

    end
end

if barg==1
    figure(17)
        bary=[-1,0,1.8,5,50];
        barx=categorical({'No Wnt-10b','Normal Wnt-10b',...
            'Wnt-10b increase 1','Wnt-10b increase 2',...
            'Wnt-10b increase 3'});
        bar(barx,bary)
        ylabel('Wnt-10b (Fold Change)','FontSize',12)
    if savegraphs==1
        saveas(figure(17),'BarFold','png')
    end
end



%% Functions needed to produce graphs
%% History functions for the DDE
function historyV1 =history1(t,y0,k,xdata,oldsol,kM)

historyV1=y0'; % Initial conditions in vector
if t<0
    historyV1(1)=200;
```

```
220 else
221     historyV1(1)=180;
222 end
223
224
225 end
226 function historyV2 =history2(t,y0,k,xdata,oldsol,kM)
227
228 historyV2=deval(oldsol,t); % Initial conditions in vector
229 %Refers to function that already resets for next time interval
230 % if t<0
231 %     historyV2(1)=200;
232 % else
233 %     historyV2(1)=180;
234 % end
235
236
237 end
238 %% Define ODE equations with variable parameters
239 function dydt= ddefun(t,y,Z,y0,k,x,oldsol,kM)%x is a scalar ...
        wnt10b dose
240
241 Bone=1;
242 alpha_1=0.5;
243 alpha_2=0.1;
244 alpha_3=0.1;
245 beta_1=0.1;
246 delta=0.1;
247 beta_2=0.1;
248 alpha_4=0.1;
249 K_S=200;
250 k1=.69825;
251 k2=0.015445;
252 g_31=1;
253 g_21=2;
254 g_22=1;
255 g_32=1;
256 g_41=1;
257 g_42=1;
258 g_43=-1;
259 g_44=1;
260 f_12=1;
261 f_14=1;
262 f_23=1;
263 f_34=1;
264 epsilon=1;
265 beta_3=0.1;
266 rho=20;
267
268     S =y(1);
269     P =y(2);
270     B =y(3);
271     C =y(4);
272     z=y(5);
```

```
273     ylag=Z(:,1);
274     Blag=ylag(3);
275
276
277     %Set parameter definitions
278     beta1adj = k(1);
279     beta2adj = k(2);
280     k2adj=k(3);
281
282     %Setting k2 relationship to wnt
283     knew=k2+((k2adj*x)/(x+kM));
284
285
286     %Algebraic equations needed for the ODEs
287     Differentiation_of_Osteoblast_to_Osteocytes = Bone*alpha_1*...
288         power(B,g_31)*max((1-S/K_S),0);
289     Differentiation_of_MSC_cells_to_PreOsteoblast_cells = Bone*...
290         alpha_2*power(S,g_21)*max((1-S/K_S),0)^g_22;
291     Proliferation_of_preosteoblasts = Bone*alpha_3*power(P,g_32)...
292         *max((1-S/K_S),0);
293     Differentiation_of_PreOsteoblast_to_mature_osteoblast = Bone*...
294         (beta_1+(beta1adj*x))*power(P,f_12)*power(C,f_14);
295     Apoptosis_of_preosteoblast = Bone*delta*P;
296     Apoptosis_of_osteoblasts = ...
            Bone*(beta_2-(beta2adj*x))*power(B,f_23);
297     Differentiation_of_preosteoclast_to_osteoclasts = Bone*alpha_4...
298         *power(S,g_41)*power(P,g_42)*power(epsilon+B,g_43)*...
299         max((1-S/K_S),0)^g_44;
300     Apoptosis_of_osteoclasts = Bone*beta_3*power(C,f_34);
301     Resorption_of_bone = Bone*k1*C;
302     Formation_of_bone = Bone*((knew*Blag));
303
304     %ODEs
305
306     %d([Osteocytes (S)])/dt = 1/Bone*
307     %Differentiation_of_Osteoblast_to_Osteocytes;
308     dydt(1)=1/Bone*Differentiation_of_Osteoblast_to_Osteocytes;
309
310     %d([Pre-Osteoblasts (P)])/dt = 1/Bone*
311     %(Differentiation_of_MSC_cells_to_PreOsteoblast_cells +
312     %Proliferation_of_preosteoblasts -
313     %Differentiation_of_PreOsteoblast_to_mature_osteoblast -
314     %Apoptosis_of_preosteoblast)
315     dydt(2)=1/Bone*...
316         (Differentiation_of_MSC_cells_to_PreOsteoblast_cells...
317         + Proliferation_of_preosteoblasts - ...
318         Differentiation_of_PreOsteoblast_to_mature_osteoblast...
319         - Apoptosis_of_preosteoblast);
320
321     %d([Osteoblasts (B)])/dt = 1/Bone*
322     %(-Differentiation_of_Osteoblast_to_Osteocytes +
323     %Differentiation_of_PreOsteoblast_to_mature_osteoblast -
324     %Apoptosis_of_osteoblasts)
325     dydt(3)=1/Bone*(-Differentiation_of_Osteoblast_to_Osteocytes...
```

```
326         + Differentiation_of_PreOsteoblast_to_mature_osteoblast...
327         - Apoptosis_of_osteoblasts);
328
329     %d([Osteoclasts (C)])/dt = 1/Bone*
330     %(Differentiation_of_preosteoclast_to_osteoclasts - ...
           Apoptosis_of_osteoclasts)
331     dydt(4)=1/Bone*(Differentiation_of_preosteoclast_to_osteoclasts...
332         - Apoptosis_of_osteoclasts);
333
334     %d([Bone volume (z)])/dt = 1/Bone*(-Resorption_of_bone +
335     %Formation_of_bone)
336     dydt(5)=1/Bone*(-Resorption_of_bone + Formation_of_bone);
337
338
339     dydt=[dydt(1)
340           dydt(2)
341           dydt(3)
342           dydt(4)
343           dydt(5)];
344
345 end
346
347 %% Solve ODE using variable parameters
348 function yout = Graham2013(k,xdata,y0,N,cyclelength,tlag,kM)
349
350     for i = 1:length(xdata)
351
352         [~,ycalc] = ...
               Cyclefunction(k,xdata(i),y0,N,cyclelength,tlag,kM);
353
354         yBV(i,1)=ycalc(end,5);
355         yout(i,1)=yBV(i,:)-100;
356
357
358     end
359     yout = yout';
360 end
361 %% Cycle Function
362      function [combined_tcalc_N_cycles, combined_ycalc_N_cycles] ...
           = ...
363          Cyclefunction(k,xdata,y0,N,cyclelength,tlag,kM)
364      startindex=1; %Indices are used to combine the loops into a
365                    %single column
366      finalindex=1;
367      oldsol=[];
368           for j= 1:N
369              tspan = [(j-1)*cyclelength,j*cyclelength];
370              if j==1
371                 %Uses initial condition vector as history
372                 sol = dde23(@ddefun,tlag,@history1,tspan,[],y0,k,...
373                     xdata,oldsol,kM);
374                 oldsol=sol; %saves solution as a history solution
375              else
376                 %Uses history solution as history function
```

```
377                 sol = dde23(@ddefun,tlag,@history2,tspan,[],y0,k,...
378                     xdata,oldsol,kM);
379                 oldsol=sol; %saves solution as a history solution
380             end
381             tcalc=sol.x';
382             ycalc=sol.y';
383             ycalc(:,1);
384             %Reset for next time interval
385             y0=ycalc(end,:);
386             idx=(y0<1);
387             y0(idx)=0; %Sets fractions of cells to zero
388             y0(1,1)=y0(1,1)-20; %Reduces osteocytes to initate ...
                    next cycle
389             oldsol.y(:,end)=y0';
390             finalindex=finalindex+length(tcalc)-1;
391             combined_tcalc_N_cycles(startindex:finalindex,1)=tcalc;
392             combined_ycalc_N_cycles(startindex:finalindex,:)=ycalc;
393             startindex=startindex+length(tcalc)-1; %equals ...
                    previous final
394                                                    %index
395         end
396
397     end
```

VITA

Carley V. Cook

Candidate for the Degree of

Master of Science

Thesis: MATHEMATICAL MODELING OF THE EFFECTS OF WNT-10B ON BONE METABOLISM

Major Field: Chemical Engineering

Biographical:

Education:

Received a Bachelors of Science in Chemical Engineering at Oklahoma State University in May 2019.
Completed the requirements for the degree of a Master of Science with a major in Chemical Engineering at Oklahoma State University in December 2020.

Experience & Honors:

OSU Graduate Research Assistant 2019-2020
Eastern Oklahoma Technology Center Chemistry Tutor 2019
OSU ChE Grader 2018-2019
Undergraduate Research Assistant 2017-2019
OSU Women's Faculty Research Award 2020
OK-LSAMP Scholar 2018-2019
Niblack Research Scholar 2018-2019
Oklahoma State Regents for Higher Education Academic Scholar 2015-2019

Professional Membership:

American Institute of Chemical Engineers (AIChE)
Society of Women Engineers (SWE)
American Indian Science and Engineering Society (AISES)